



A critical review on renewable battery thermal management system using heat pipes

Asif Afzal¹ · R. K. Abdul Razak² · A. D. Mohammed Samee² · Rahul Kumar³ · Ümit Ağbulut⁴ · Sung Goon Park¹

Received: 14 November 2022 / Accepted: 12 March 2023 / Published online: 2 May 2023
© Akadémiai Kiadó, Budapest, Hungary 2023

Abstract

The critical review presented here exclusively covers the studies on battery thermal management systems (BTMSs), which utilize heat pipes of different structural designs and operating parameters as a cooling medium. The review paper is divided into five major parts, and each part addresses the role of heat pipes in BTMS categorically. Experimental studies, numerical analyses, combined experimental and numerical investigations, optimum utilization of a phase-change material (PCM) with a heat pipe (HP), oscillating heat pipe (OHP), and micro heat pipes combined with PCM for Li-ion BTMS using heat pipes are presented. The usage of HP's and PCM can keep the temperature of the battery system in the desirable limit for a longer duration compared to other traditional and passive methods. More emphasis is made on how one can achieve a suitable cooling system design and structure, which may tend to enhance the energy density of the batteries, improve thermal performance at maximum and minimum temperature range. Arrangement of battery cells in a pack or module, type of cooling fluid used, heat pipe configuration, type of PCM used, working fluid in a heat pipe, and surrounding environmental conditions are reviewed. According to the study, the battery's effectiveness is significantly influenced by temperature. The usage of flat HPs and heat sink proves to be the best cooling method for keeping the battery working temperature below 50 °C and reduces the heat sink thermal resistance by 30%. With an intake temperature of 25 °C and a discharge rate of 1 L per minute, an HP that uses water as a coolant is also effective at regulating battery cell temperature and maintaining it below the permissible 55 °C range. Using beeswax as a PCM in HPs reduces the temperature of BTMS by up to 26.62 °C, while the usage of RT44 in HPs reduces the temperature of BTMS by 33.42 °C. The use of fins along with copper spreaders drastically decreases the temperature capability of HPTMS by 11 °C. MHPA shows excellent performance in controlling the battery temperature within 40 °C. The effective thermal management can be done by incorporating heat pipe alone or by coupling with liquid cooling or metal plate. However, extensive and extended research is required to improve thermal management to safely and effectively use the battery for day-to-day applications.

Keywords Cylindrical battery cells · Electric vehicle · Heat pipes · Lithium-ion battery · Phase-change materials · Thermal management

Abbreviations

ADI	Alternating direction implicit
Ar	Aspect ratio
CFD	Computational fluid dynamics
C_m	Average skin friction coefficient
FDM	Finite difference method
FEM	Finite element method
FVM	Finite volume method
H	Heat transfer coefficient
HP	Heat pipe
HT	Heat transfer
K	Conductivity
L	Dimensionless distance of fuel element.
Nu	Average Nusselt number
NU	Nonuniform heat generation

✉ Sung Goon Park
psg@seoultech.ac.kr

¹ Department of Mechanical and Automotive Engineering, Seoul National University of Science and Technology, Seoul, South Korea

² Department of Mechanical Engineering, PA College of Engineering, Mangalore, India

³ Department of Mechanical Engineering, National Institute of Technology, Srinagar, India

⁴ Department of Mechanical Engineering, Faculty of Engineering, Düzce University, 81620 Düzce, Turkey

Pr	Prandtl number
Qt	Total energy generation parameter when only solid domain was considered
Re	Reynolds number
To	Maximum allowable temperature of battery cell
U_{∞}	Free stream velocity
V	Velocity component in Y direction
x	Axial coordinate
X	Dimensionless axial coordinate
Y	Dimensionless transverse coordinate

Greek symbols

θ	Dimensionless maximum temperature
Sf	Solid–fluid interface
∞	Free stream
μ	Dynamic viscosity
α	Thermal diffusivity of fluid
N	Kinematic viscosity of fluid
P	Density of fluid

Introduction

Net zero is important because it is the best strategy to combat climate change by bringing down global temperatures. The future will depend on what we do to limit emissions during the coming ten years, so every nation, business group, and individual must work together to identify strategies to lower the amount of carbon that we produce [1]. Additionally, the COVID-19 pandemic has resulted in lessened air and noise pollution, which has improved the environment all over the world. This unexpected advantage suggests that renewable and sustainable energy sources are the way of the future. The disastrous impact of fossil fuels on air pollution and fossil fuel scarcity prompted scientists to establish numerous forms of low-carbon energy transport systems [2, 3]. Especially petrol, which is linked to international security, is more evident due to unequal distribution and yearly rise in its consumption [4]. Overall, private transport is 80% oil-dependent and is responsible for more than 40% of world oil utilization [5, 6]. Vehicle-exhausted contaminants like NO_x, dust, and CO₂, have been the primary causes of fog and haze [7].

Electric vehicles (EVs) and hybrid electric vehicles (HEVs) have received a lot of interest in the world in recent years because of their ability to lower pollution [8, 9]. The power battery is the main factor constricting its performance [10], and the safety of batteries is a crucial concern for their utilization. Even the prices for both suppliers and consumers should be taken into account [11]. Since the introduction of li-ion battery in 1991, it has gained huge interest compared to other types of rechargeable batteries. The advantages of li-ion batteries include their high energy and power density,

low self-discharge rate, and high voltage [12, 13]. The operating temperature of the lithium-ion batteries (LIBs) has a significant impact on its longevity [14, 15].

As batteries are chemical power sources, strong chemical reactions occur during charging and discharging and release large quantities of heat, increasing the chemical reaction rate. Rapidly increasing overall battery temperature and worsening nonuniform temperature will severely affect its lifespan, capacity, safety, etc. Research has shown that battery lifetime decreases by approximately 60 days when the battery temperature rises by 1 °C in the 30–40 °C range [16]. Additionally, mechanical abuse, short circuit, excessive heat, and overloading are likely to cause thermal runaways and induce safety accidents. Besides this, the battery output will deteriorate as the lithium-ion diffusion power decreases at low ambient temperatures [17]. Hence, effective battery thermal management system (BTMS) is imperative for the li-ion battery to obtain optimum battery efficiency [18, 19].

Battery thermal management system (BTMS)

Based on the analysis, two significant problems arise due to temperature. The first one is that the excess temperature during charging and discharging causes temperatures to exceed acceptable levels and reduce battery life. The second one is that the unequal temperature distribution within the battery system will result in localized deterioration. To ensure that the cell, module, and pack attain their full cycle life, temperature consistency is vital [20]. Therefore, to enhance the efficiency of batteries or battery packs, thermal energy management systems (BTMSs) must be integrated with them.

In order to achieve the full cycle life of the cell, module, and pack [20], temperature uniformity is necessary. Hence to enhance the efficiency of a battery module, the BTMS must be fitted with battery packs. They assist the battery in executing at the favorable working temperature range at all periods restraining battery deterioration [21, 22], thermal runaway [23, 24], and decreased discharge capacity owing to extreme cold climate [25]. The installed BTMS should have good performance characteristics along with light weight [26, 27]:

- Optimum operational range of temperature for each cell as well as for all battery modules, heat removal in hot environments/heat addition in cold environments.
- Minimal differences in cell temperature and module temperature.
- Low variations in temperature between different modules.
- Compact and portable, simple to carry, durable, reduced cost, and system-friendly.
- A ventilation arrangement if the battery produces hazardous gases.

Thermal management techniques may be in-built or external. Further investigation is required to determine whether the integrated BTM in li-ion batteries can improve temperature uniformity within and among cells in a package [28, 29]. External BTMSs are most exhaustively used and will be described here. This can be classified as passive (only ambient air is utilized for cooling) or active (an integrated source is used for heating or cooling), or depending on the medium (1) air cooling [9, 30, 31], (2) liquid cooling [32–34], (3) cooling using PCM materials [35–37], (4) cooling using nanofluids [36–42] (5) cooling using heat pipe, and (6) combination of above methods. BTMS categorization based on the cooling agent is displayed in Fig. 1. [43].

Heat pipes (HPs)

Heat pipes are widely used as temperature control devices for many residential and commercial systems. This is attributed to their prominent features of high total heat conductivity. They are indeed known as "thermal superconductors" [44, 45] because their total heat conductivity can be as much as ninety times larger than a copper rod of similar dimensions. At nearly constant temperatures, they can keep the evaporator surface uniform. Furthermore, the geometry of

this system is adaptable to a wide range of spaces. HP is a good option for cooling and refrigerating HEV/EV batteries because of its appealing features [46, 47].

A HP is a 2-phase heat transfer (HT) system used to transfer a significant quantity of heat with a slight temperature gradient. Actually, it plays the role of a "superconductor" in transmitting heat from one system to another in diverse applications without or with the least heat loss. There are two main advantages of choosing a heat pipe: (1) No additional system is required to pump the coolant into the HP and (2) HP is a 2-phase HT system with a relatively high coefficient of heat transfer as contrasted with a single-phase heat transfer system [48, 49]. Therefore, it will transfer a large quantity of heat.

As displayed in Fig. 2, a HP comprises of a tubular metal frame closed on both sides. It basically comprises three key components, namely the evaporator, adiabatic component, and condenser. The operating fluid moves into this heat pipe in both liquid and vapor forms. Therefore, when an evaporator component is affected by a temperature source, the liquid vaporizes, absorbs, and captures a significant quantity of heat [50, 51]. Then, the vapor (shown by red downward arrows) flows into the condenser, raising the vapor pressure. In the condenser section, the vapor is then changed into

Fig. 1 BTMS categorization based on cooling agent [43]

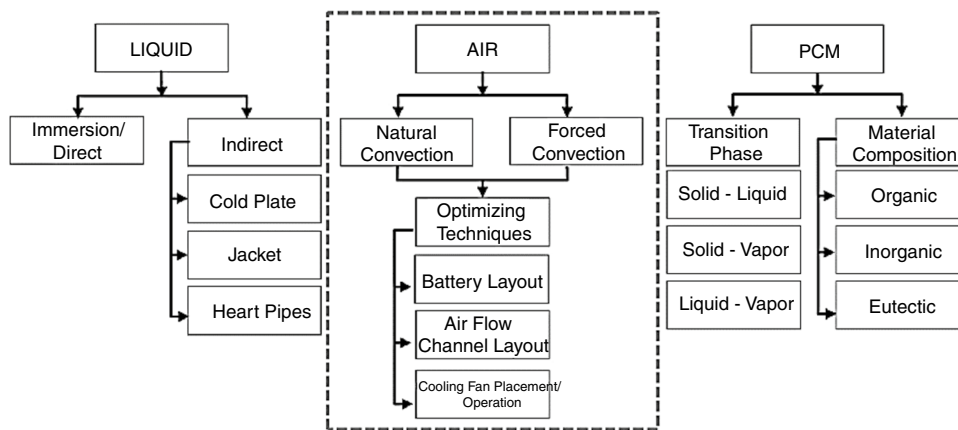
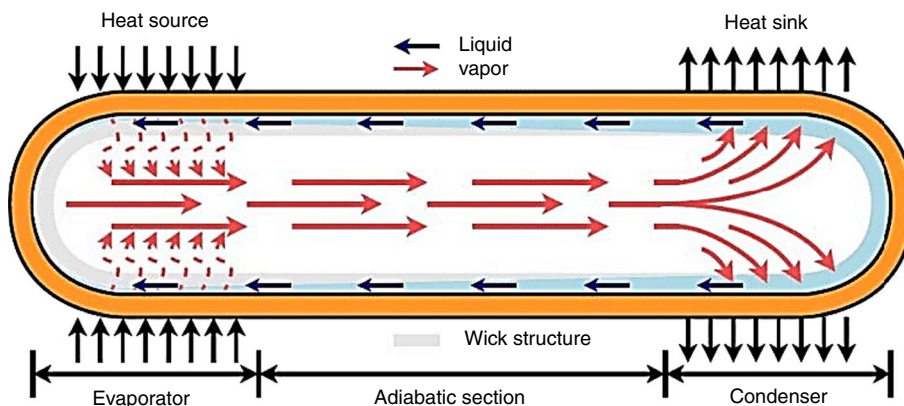


Fig. 2 Illustration of the heat pipe [53]



liquid, releasing the latent heat. The heat sink absorbs this heat. Actually, heat is extracted in the condenser by cooling a circuit that may be based on air or water. The condensate returns back to its initial position in the wick structure indicated in gray by the capillary action [52, 53].

HP applications

HPs can be used in a variety of applications, including [54, 55]:

1. Compact Electronics Enclosures
2. Aerospace
3. Medical
4. Consumer Electronics
5. HVAC

Compact electronics enclosures

Compact electronics enclosures are often operated in situations considerably beyond their survivability temperature limits and with insufficient heat sinks. Using HP and HP-based technologies, a thermal management system for electronics cooling in high temperature avionics situations has been used from many decades. The system lowers the inefficiencies in thermal energy transport inside electronics enclosures, detects possible sinks to offer continuous heat rejection across the platform's operational environment, and delivers passive thermal energy transport from the electronics enclosure to chosen sinks. Hence, they provide a highly efficient, portable cooling setup for electronic cabinets and enclosures and also fulfills today's increasing demand for thermal power requirements due to higher miniaturization [56].

Aerospace

HP is an attractive feature in the aerospace sector for spacecraft freezing and temperature stabilization due to its low weight, lesser maintenance costs, and consistent functions. Managing aerospace isothermal components is a critical task with regard to obituary astronomy practices under harmful solar heating.

By transferring heat from the Sun-facing side to the cold side, HPs have been used to control the temperature of spacecraft structures and maintain a more consistent temperature throughout the spacecraft. This is caused by the spacecraft's exposure to intense solar radiation on one side and the chilly vacuum of space on the other. The heat produced by the electronic systems in satellites has also been dissipated via heat pipes [57]. In sounding rockets, early heat pipe studies for aeronautical applications were carried

out. Experiments with HP's employing an ammonia HP with a spiral arterial wick were conducted on the application technology satellite-6 [58]. Flight testing of HP designs was done on a massive scale using the space shuttle [59]. In order to assess the starting behaviour and transport capacities during microgravity exercises, NASA and the US Air Force tested two distinct axially grooved oxygen heat pipes onboard the Shuttle Discovery (STS-53) in 1992 [60].

Consumer electronics

Heat pipes and heat exchangers are mainly useful in day-to-day consumer-specific electronic equipment such as power supplies, laptops, desktop computers, and microprocessors. All these electronic equipments produce heat, and the removal of this heat is essential for the efficient and dependable functioning of these components. Managing the heat load becomes a crucial design consideration when electronic architecture enables better throughput in smaller packaging. More cooling is needed for many modern electronic equipment that can be provided by typical metallic heat sinks. The heat pipe is quickly replacing other thermal management methods since it fulfills this necessity. Since the early 1960s, heat pipes have been available on the open market. The electronics sector has only recently accepted heat pipes as dependable, economical options for high-end cooling applications [61].

Medical

Thermal problems impose a limit on the system's overall performance and dependability in an expanding number of healthcare device applications. The use of simple thermal management techniques such liquid cold plates, air-cooled heat sinks, and thermal interface elements is no longer adequate. Implementing cutting-edge thermal technology like heat pipes and vapor chambers is becoming a crucial component of the thermal management strategy in many new medical technologies. Excellent heat transmission and heat spreading capabilities are provided by these technologies. They are also reliable, quiet, and passive (no energy or moving components). They provide useful benefits in terms of reducing area, decreasing weight, and minimizing maintenance costs, resulting in fewer environmental impacts compared to other cooling devices based on different technologies like pumped liquids, etc. These technologies are already used in a number of medical equipment, including powered surgical forceps, skin/tissue contacting tools, and polymerase chain reaction (PCR)/thermo cyclers, and new applications are constantly being developed [62].

HVAC

It is well known that a HP heat exchanger is used for heat recovery in both hot and cold regions. Because of the minimal pressure drop provided by the HP exchanger using loop arrangements, heat recovery operations may be expanded to drier areas while still being economical. Summertime “cooling” recuperation is a novel potential that is now financially viable enough to be taken into account. One of the most alluring uses is the use of HP as a heat exchanger to recover lost heat and increase the capacity of a traditional cooling coil to remove moisture. The relative humidity of the air may be reduced by 10% using HP heat exchangers, which results in a notable improvement in the quality of fresh air and a reduction in energy consumption. The heat pipe is an innovative device that has the potential to improve fresh air quality while also contributing to energy conservation [63].

Advantages of using heat pipes

Heat pipe, popularly known for its high effective heat transfer due to phase change, has recently gained more attention for high-efficiency BTMSs for the following reasons [44, 64, 65].

1. It not only possesses high thermal conductivity, energy efficient, robust construction, long service life, and high reliability, but it also has specific two-directional features. (Evaporator and condenser can be swapped based on overall cooling/heating requirements)
2. Smaller HPs are preferred in BTMS due to the additional advantages of a more robust and lightweight framework, as well as more efficient construction, to meet the requirements for constrained space and compactness in EVs.

The various other advantages of heat pipes are as follows [66, 67]:

- A superconductor to transmit heat energy to various applications without or least heat loss with reliable heat distribution.
- Better performance compared to the copper rod (the most well-known conductor) in heat transfer.
- Less maintenance
- Transmittance of a substantial volume of heat energy with a low-temperature differential to the heat pipe surface.

Mathematical models

Due to the differences in shape, chemical composition, and required level of accuracy, different battery types (such as

prismatic, cylindrical, and pouch) require different modelling approaches. A module's battery configuration can also have an impact on the mathematical modelling process. The modelling process is shown in Fig. 3. The partial differential equations regulating the transfer of heat, and the fluid flow of cylindrical and prismatic battery cells is given below.

The various equations required to be solved to do the numerical solution on the prismatic type of battery cells (both conjugate, non-conjugate, transient, and steady-state HT and fluid flow problems) are given below:

A prismatic battery's energy conservation formula is given by [69]

$$\rho C_p \frac{\partial T}{\partial \tau} = \frac{\partial}{\partial x} \left(\lambda_x \frac{\partial T}{\partial x} \right) + \frac{\partial}{\partial y} \left(\lambda_y \frac{\partial T}{\partial y} \right) + \frac{\partial}{\partial z} \left(\lambda_z \frac{\partial T}{\partial z} \right) + q \tag{1}$$

where ρ stands for density, C_p —specific heat, $\lambda_x, \lambda_y, \lambda_z$ —heat conductivity in the x, y, z direction, and q —volume heat production rate.

The volumetric heat production rate ‘ q ’ is determined from the overall battery heat production ‘ Q ’ divided by battery volume V , shown as

$$q = \frac{Q}{V} \tag{2}$$

The ‘ q ’ constitutes ohmic heat, irreversible and reversible heat [70] given by.

$$Q = I(E_{oc} - U) - IT \frac{dE_{oc}}{dT} \tag{3}$$

Coolant model (Cartesian and polar)

The equations governing the coolant's behavior under the assumption that water is an incompressible coolant are as follows [71] (Fig. 4):

$$\rho_c \frac{\partial T_c}{\partial \tau} + \nabla \cdot (\rho_c \vec{v} T_c) = \nabla \cdot \left(\frac{k_c}{c_c} \nabla T_c \right) \tag{4}$$

$$\rho_c \frac{dv}{d\tau} = -\nabla p + \mu \nabla^2 v \tag{5}$$

$$\frac{\partial}{\partial t} (\rho h) + \frac{\partial}{\partial x_i} (\rho u_i h) = \frac{\partial}{\partial x_i} \left(K \frac{\partial T}{\partial x_i} \right) \tag{6}$$

The continuity, momentum, and energy equation given in [35, 73–75] are the unsteady governing equations used to investigate transient, 3-dimensional heat & flow problems linked to cylindrical battery packs.

Continuity equation

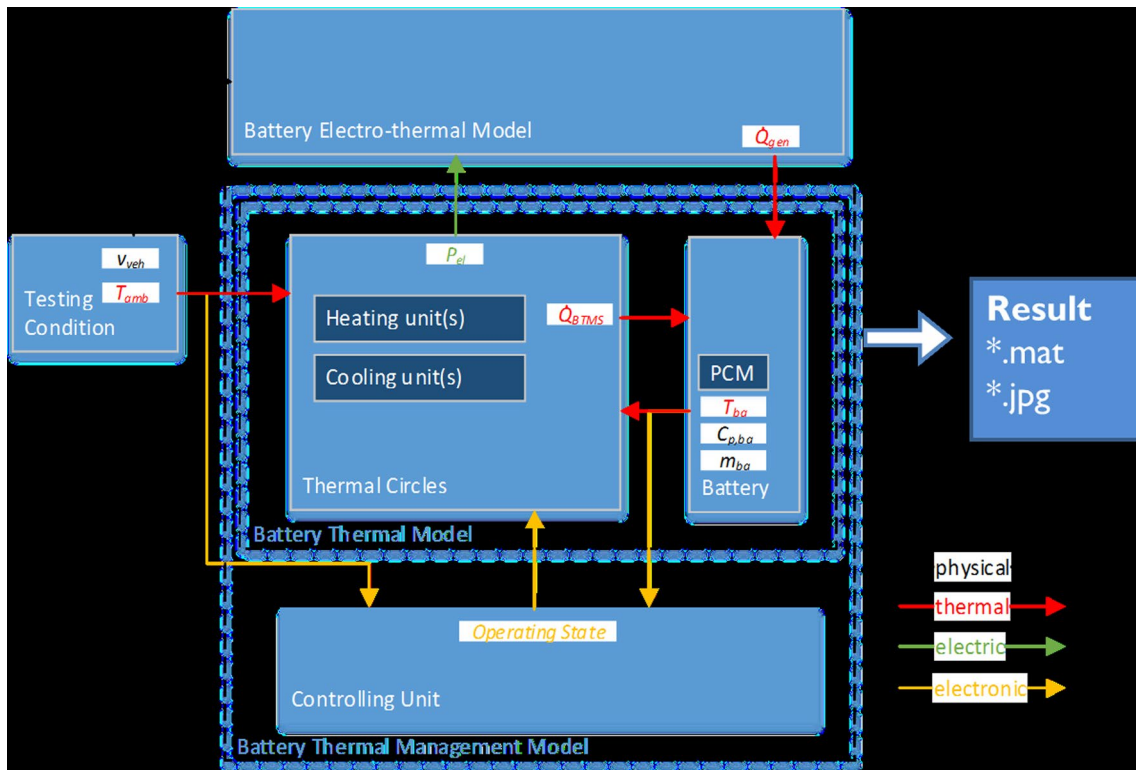


Fig. 3 Modelling process of BTMS (an example) [68]

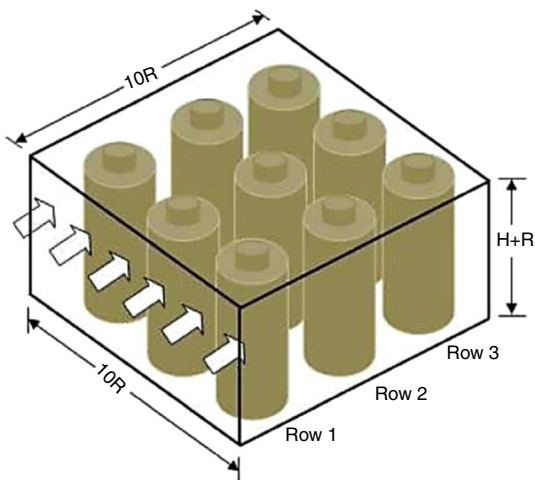


Fig. 4 A transverse depiction of a battery system showing the air flow in a specific direction [72]

$$\frac{\partial \rho}{\partial \tau} + \nabla \cdot (\rho \hat{u}) = 0 \tag{7}$$

X-momentum

$$\frac{\partial(\rho u)}{\partial \tau} + \nabla(\rho u \hat{u}) = -\frac{\partial P}{\partial x} + \nabla \cdot (\mu \nabla \hat{u}) + S_{mx} \tag{8}$$

Y-momentum

$$\frac{\partial(\rho v)}{\partial \tau} + \nabla \cdot (\rho v \hat{u}) = -\frac{\partial P}{\partial y} + \nabla \cdot (\mu \nabla v) + S_{my} \tag{9}$$

Z-momentum

$$\frac{\partial(\rho w)}{\partial \tau} + \nabla \cdot (\rho w \hat{u}) = -\frac{\partial P}{\partial z} + \nabla \cdot (\mu \nabla w) + S_{mz} \tag{10}$$

Energy Equation

$$\frac{\partial}{\partial t}(\rho h) + \frac{\partial}{\partial x_i}(\rho u_i h) = \frac{\partial}{\partial x_i} \left(K \frac{\partial T}{\partial x_i} \right) \tag{11}$$

And for the battery pack, the formula is given by [76]:

$$\rho_b C_{pc} \left[\frac{\partial T}{\partial t} \right] = k_s \left[\frac{\partial^2 T}{\partial x^2} + \frac{\partial^2 T}{\partial y^2} + \frac{\partial^2 T}{\partial z^2} \right] + q_g \tag{12}$$

where q_g denotes the quantity of heat produced within the battery pack (BP) and is given as

$$q_g = q_e e + q_{oh} \tag{13}$$

q_e is entropic heating, and q_{oh} is ohmic heating

Heat pipe (HP) model

The internal flow of the HP is described by the equation below [77]:

$$\Delta p_c \geq \Delta p_v + \Delta p_l + \Delta p_g \tag{14}$$

where the peak capillary pressure is Δp_c ; Δp_v and Δp_l are the pressure losses created by the flow of liquid and vapor within the HP. Δp_g is the gravity-caused pressure loss.

As per the Young–Laplace theorem, Δp_c can be determined as [78]:

$$\Delta p_c = \frac{2\sigma}{r_c} \tag{15}$$

Here, r_c is the capillary radius, referring to the liquid's surface tension.

The method used to calculate the pressure losses brought on by liquid, vapor, and gravity flow is [78]:

$$\Delta p_l = \frac{\mu_l L_e^0 \nu}{KA_w \rho_l^0 H_l} \tag{16}$$

$$\Delta p_v = \frac{32\mu_v L_e \nu}{d_h^2 A_v \rho_v^0 H_l} \tag{17}$$

$$\Delta p_g = \rho_l g(z_2 - z_1) = \rho_l g z_c \tag{18}$$

Here, μ —dynamic viscosity; A —area of HP; ρ —density; the subscripts l , v , and w refer to the liquid, vapor, and wick, respectively. L_e —HP effective length, d_h —vapor space hydraulic diameter, K —permeability of the wick, H_l —liquid latent heat of the, and z_c —effective capillary height.

The following equations can be used to calculate the wick features [79]:

$$k_w = \frac{k_l [(k_1 + k_c) - (1 - \epsilon)(k_1 - k_c)]}{[(k_1 + k_c) + (1 - \epsilon)(k_1 - k_c)]} \tag{19}$$

$$\rho_{wick} = \epsilon \rho_l + (1 - \epsilon) \rho_c \tag{20}$$

$$c_{wick} = \frac{\epsilon \rho_l C_l + (1 - \epsilon) \rho_c C_c}{\rho_w} \tag{21}$$

Here, k —thermal conductivity, ρ — density, C —specific heat capacity, ϵ —porosity of wick. The symbols l and c denote liquid and sintered copper powder, respectively.

Types of HPs used for BTMS

Various kinds of HPs used for BTMS are as follows:

1. Loop heat pipe (LHP)
2. Oscillating or pulsating heat pipes

LHP

The LHP is a simple mechanism that helps the HT move from one location to another. LHPs are frequently referred to as “super thermal conductors” because of their exceptionally good thermal conductivity under steady-state conditions, which is the main benefit of using them over conventional methods. As shown in Fig. 5, a typical conventional LHP consists of an evaporator, condenser, liquid line, and compensation chamber. The fluid vaporizes in the evaporator (hot part), releasing energy as latent heat, which is then condensed in the condenser (cool part). Capillary or pump forces, for example, maintain the liquid's circulation. The typical evaporator configuration is cylindrical, and flat evaporators are thought to reduce thermal resistance between the heat source and the evaporator [80, 81].

Oscillating heat pipes (OHPs) or pulsating HP (PHP)

OHP, or PHP, is the recent developments in HP technology. They are made up of a lengthy, winding tube that is heated and cooled at various points along its length and were first designed and patented by Akachi in 1990. The working fluid oscillation theory and the capillary tube phase change process serve as the foundation for the working of OHPs [83–85]. The tube's diameter needs to be small enough to fit plugs for vapor and liquid. OHPs can function

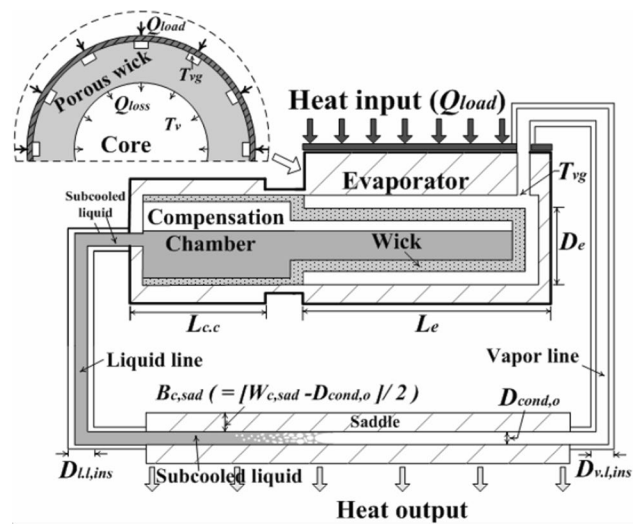


Fig. 5 Loop heat pipe model [82]

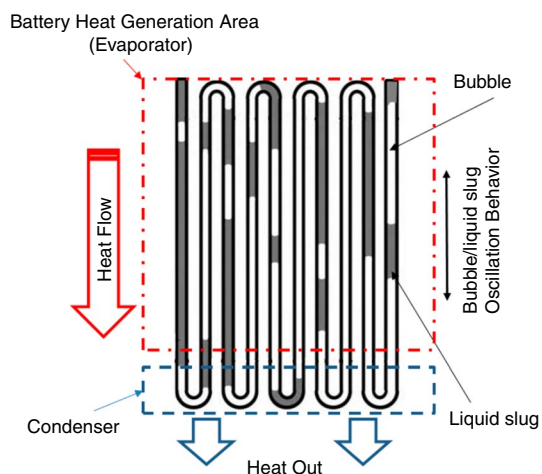


Fig. 6 Oscillating heat pipe [85]

at high thermal fluxes and, unlike conventional heat pipes, do not need a wicking system to transport the liquid [86].

A schematic of the OHP is shown in Fig. 6. An OHP is generally a meandering tube containing a capillary-dimensional serpentine channel. The OHP is drained initially and then partially replaced with the cooling medium. The influence of surface tension causes liquid slugs to form, interspersed with vapor bubbles. The operating fluid starts evaporating when heat is added to the evaporation area [88, 89]. As the vapor pressure inside the tube rises, the bubbles in the evaporator section enlarge and push the liquid in the direction of the condenser. Bubble condensation results from a decrease in vapor pressure as the condenser cools. The evaporator and condenser sections of the tube are where this continuous process oscillates. Vapor latent heat and liquid slug sensible heat are the means by which heat is transferred [90–92].

UMHPs (UltraThin Micro HPs)

These are used to minimize the upsurge in temperature of a prismatic 3.2 V50 Ah Li-ion battery pack (BP) made up of multiple parallel cells for EVs. UMHPs have been recognized as a very effective and energy-efficient system for BTMS due to the constrained space in battery packs and the compact size of EVs. UMHPs consist of a sealed tube filled with operating fluid that is saturated. In this system, the heat source causes the working fluid in the evaporator to vaporize, and the resulting vapor, with a small pressure difference, transfers the heat to the condenser. Following that, air convection is used to move the heat from the condenser to the wall [93, 94]. The capillary-enforced wick keeps this process going by ensuring that the liquid produced in the condenser is transferred back to the evaporator. Figure 7 displays a schematic of UMHPs.

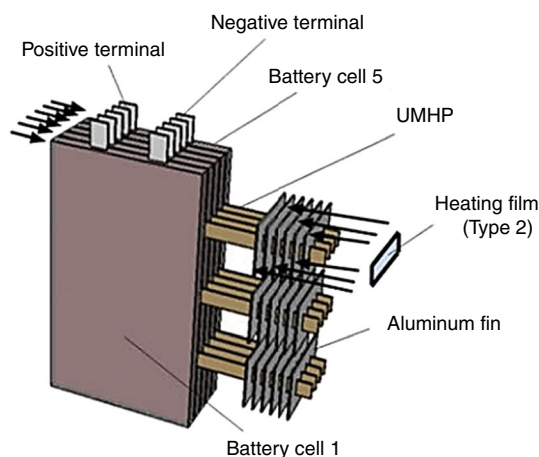


Fig. 7 UMHP BTMS [95]

Addition of HPs with PCM

PCM

HPs exhibit excellent heat transfer capability and have high heat transfer efficiency with PCMs. In addition, HPs can be integrated within PCMs to reduce thermal resistance. Other advantages of integrating HPs in a high heat storage scheme include segregating heat source and sink and regulating and controlling temperature [96]. PCM combined with heat pipe aims to merge the heat pipe's great thermal conductivity with PCM's large latent heat storage. The PCM functions as a thermal reservoir and the HP transports heat energy to the buffer and from there it is transferred to the position where it is necessary [97]. Consequently, the advantages of HPs and PCMs can be combined to resolve each other's defects. This integrated module has several uses in electrical refrigeration modules, thermal energy storage, and solar systems [98].

The design of a system with concurrent charging and discharging activities is crucial for the continuous operation of devices that use time-related energies like solar energy or other energies that are related to the passage of time and whose amounts can change. HPs and PCMs can be integrated to provide simultaneous charging and discharging. PCM provides an efficient heat-saving capability in photovoltaic/thermal modules that draws heat energy from solar panels and lowers the operating temperature of those components. Additionally, the micro ducts' heat pipe can transfer and extract heat energy to prevent photovoltaic and thermal module degradation from freezing. In a solar still with an evacuated pipe collector, employing an additional condenser augmented using PCM and combined with HPs contributes to continuous desalination without reducing the system's efficiency throughout the day [99–101].

PCMs connected with heat pumps, HPs, or both, must have high melting enthalpies and low storage densities. Figure 8a–e displays the PCM-integrated HPs.

PCMs are typically categorized into two groups: inorganic and organic. The benefits of organic PCMs include their non-corrosivity, high thermal and chemical sustainability, and minimal subcooling, whereas their drawbacks include their low melting enthalpy, low density, and extreme flammability. On the other hand, inorganic PCMs have high melting enthalpy and density but are corrosive, cycling unstable, and subcooled. These aspects should be considered when selecting these materials to pair with heat pumps or HPs. A few of the PCMs used in BTMS alone are mentioned in Table 1, along with their properties.

Motivation and organization

Lithium-ion batteries are facing technical challenges despite their numerous applications, from energy storage to electric mobility. These batteries possess several advantages, like greater energy density and smaller self-discharge. However, they are still in the developing phase, and several issues need to be fixed to improve the battery's safety and performance. Considerable research has been carried out in the past and is underway to address the battery's thermal, mechanical, and volume issues. With the evolving computational tools and experimental setups, these researches are made possible. Based on their application, a wide range of research activities are carried out to combat the thermal issues of batteries under varied conditions. BTMS, as an energy efficient and renewable energy source for pollution-free automobiles, will rule the transport sector. To enhance the battery life and thermal efficiency, various methods are reported that are too numerous to cite. Phase-change materials, plate cooling, heat pipes, structural arrangements, etc., are used for heat transfer enhancement. The use of nanofluids especially MWCNT-water nanofluid ([108–111]) and graphene nanofluids [112–114] along with PCM in BTMS has grown significantly [115].

This review article presents a critical review of BTMS and discusses the various methods and techniques used in BTMS, specifically focusing on the use of HPs and the combination of HPs with different cooling systems. The article also critically evaluates the effectiveness and efficiency of these different methods and systems. In this article, the literature studies and research conducted in the past 10 years are reviewed, with an emphasis on the important characteristics and variables taken into account during experimental and numerical investigations. Techniques for improving heat transmission, heat pipe configurations, and various cooling systems were all extensively examined for each type of heat pipe. In order to establish a strong foundation for the development of BTMS based on HPs, the paper also describes

various method researchers have used to measure temperature using both experimental and numerical methods. Additionally, recommendations for future research are given. The article will provide a summary of the current advances in this field, highlighting the most significant discoveries and patterns. Figure 9 outlines the review structure for the present study.

Experimental BTMS studies with heat pipes

In this section, the recent experimental studies carried out on BTMS using only heat pipes are reviewed. It will be helpful for the researchers who want to carry out their research on BTMS using experimental methods with the aid of heat pipes. Wo et al. [116] experimentally conducted a 2-D transient heat transfer analysis of a BP connected to heat pipes at its outer surface. Temperature upsurge on battery surface for various flow rates were studied. A cooling fan is fixed to HP condenser unit. The results obtained from the study clearly show that using heat pipes and Aluminum fins diminishes the temperature upsurge in battery cells, which helps in stable temperature pattern. Rao et al. [117] presented an experimental work on heat pipes used for improving the life, design, temperature limit, and power generating capacity of Li-ion batteries. The HPs make use of a wick soaked with water as a cooling fluid. The rate at which heat is generated within the battery pack or module on battery temperature increase was examined under unsteady heat transfer conditions. They found that for the power input of 50W, the temperature within the battery can be kept under 50 °C, while for the input power of 30W, the temperature difference was around 5 °C.

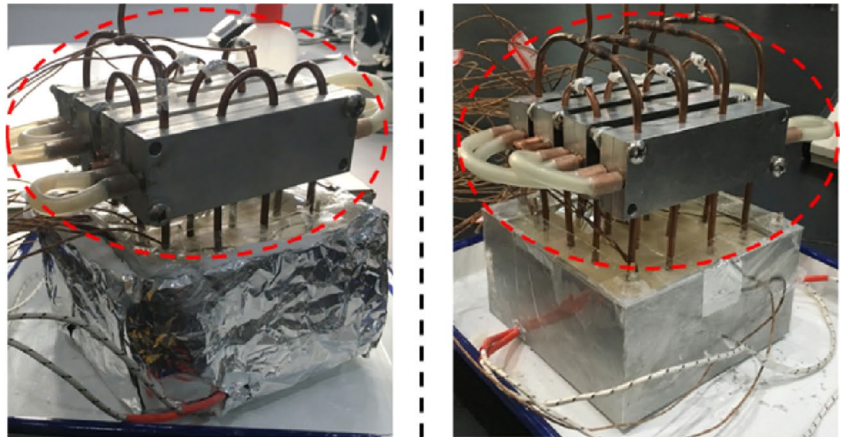
In the power batteries, the average generation rate of heat is given by Eq. (22) [118]:

$$H_{\text{avg}} = \frac{h_{\text{total}}}{t'} \quad (22)$$

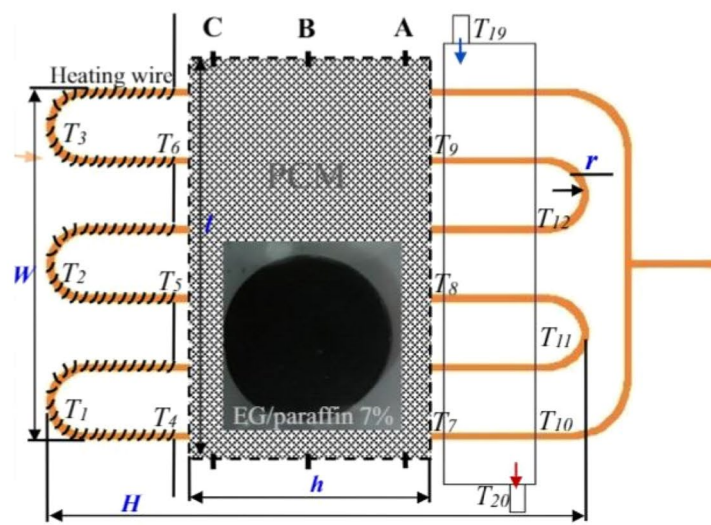
where H_{avg} is the average rate of heat generation in KW, h_{total} is heat capacity in KJ, and t' is time for discharge.

In order to determine the effectiveness of flat HPs in lowering the extreme temperature and temperature variation of the battery module with a heat sink in hybrid electric vehicles, Tran et al. [119] carried out an experiment (HEVs). In the experiment, the HP was placed horizontally, vertically, and at an angle. The outcomes were compared to those of active and passive cooling systems. The usage of flat HPs with a heat sink was found to be the most efficient cooling method, as it kept the battery temperature during operation below 50 °C and 30% lessened heat flow resistance in the heat sink. Wang et al. [120] proposed an experimental solution to the heating and cooling by HPs

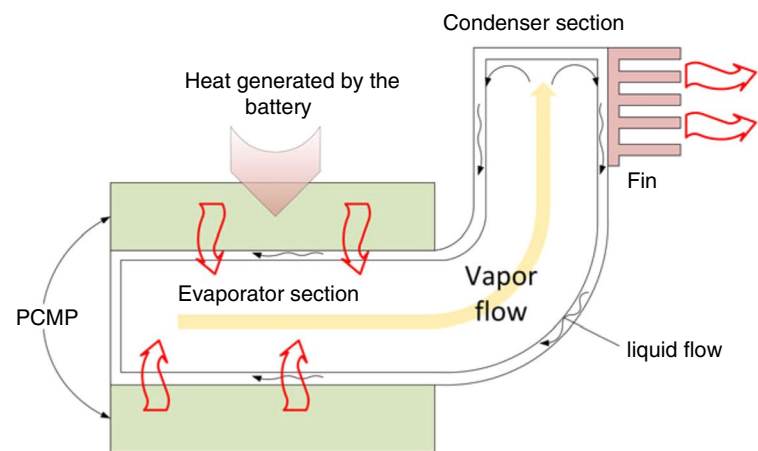
Fig. 8 Different concepts of PCMs used in BTMS integrated with heat pipes **a** OHP with PCM [87]. **b** Closed loop OHP with PCM [102]. **c** PCM-based cooling [103]. **d** PCM with HP for TM of a cylindrical power battery system [104]. **e** Finned heat pipe assisted PCM [105]. **f** Diagram of the HP-conceptual TMS's design for a BP [106]. The review outline for the present study



(a) OHP with PCM [87].

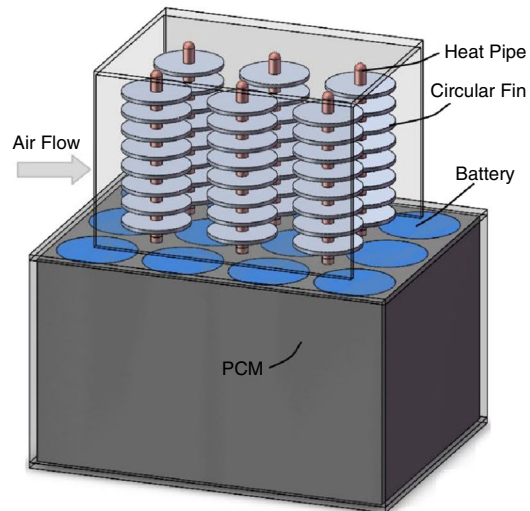


(b) Closed loop OHP with PCM [102].

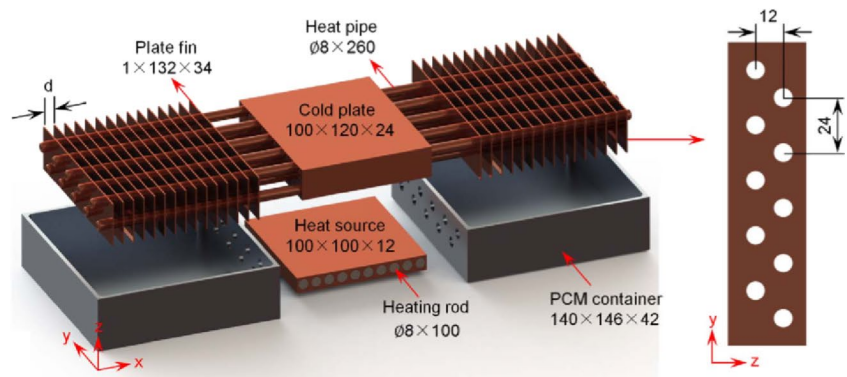


(c) PCM-based cooling [103]

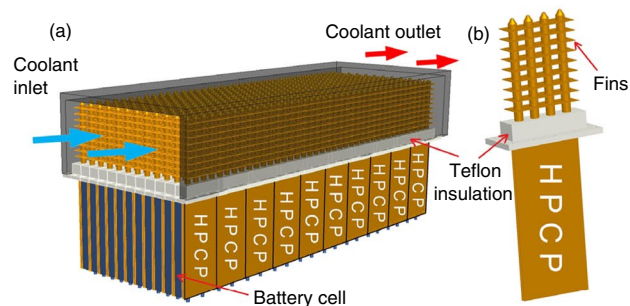
Fig. 8 (continued)



(d) PCM with HP for TM of a cylindrical power battery system [104]



(e) Finned heat pipe assisted PCM [105]

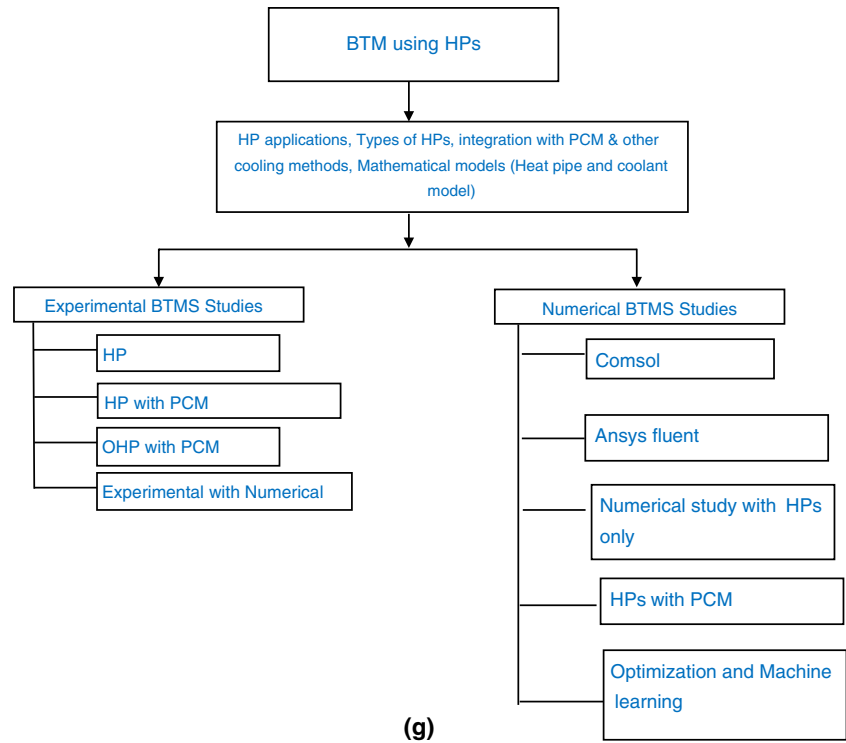


(f) Diagram of the HP -conceptual TMS's design for a BP [106]

of Li-ion batteries. Each battery cell had a power input of 10W with various flow velocities. The aim of this investigation was to maintain a secure operating temperature for the battery cell below 40 °C, prevent thermal runaway, and enhance the battery's working efficiency. The experimental findings of this research demonstrate that the use of HPs improves the uniformity of temperature in the cells and keeps the temperature of the battery cell well within 40 °C

in comparison to not using HPs. This study also depicted the recovery time required for heating battery cells from - 15 to + 5 °C, which was found to be around 300 s under 40 °C heating conditions. Through the use of HPs in an elliptical shape fixed to ribbed structures, Belyaev et al. [121] investigated the cooling efficiency of Li-ion batteries. The HP was located between the battery cells, each having a power capacity of 7.5 W, and the space between the

Fig. 8 (continued)

**Table 1** Thermal and physical characteristics of PCMs for different applications [107]

Compound	Melting temp/K	Latent heat / kJ·kg ⁻¹ K ⁻¹	Specific heat capacity/ kJ·kg ⁻¹ K ⁻¹	Thermal conductivity/ W·m ⁻¹ K ⁻¹	Density/kg/m ³
n-Octadecane	27.7	243.5	2.66 (liquid) 2.14 (solid)	0.148 (liquid) 0.190 (solid)	785 (liquid) 865
Paraffin wax (PW)	32–32.1	251	1.92(solid) 3.26(liquid)	0.514 (solid) 0.224 (liquid)	830
Capric acid	32	152.7	–	0.153 (liquid)	878 (liquid) 1004 (solid)
Lauric acid	41–43	211.6	2.27(liquid) 1.76(solid)	1.6	1.76(solid) 0.862
Paraffin RT60/RT58	55 to 60	214.4–232	0.9	0.2	775(liquid) 850(Solid)
ZnCl ₂ /KCl (31.9%/68.1%)	235	198	–	0.8	2480
P116-Wax	46.7–50	209	2.89 (liquid) 2.89 (solid)	0.277 (liquid) 0.140 (solid)	786 (solid)

cell wall and the HP was coated with a thermal-conducting paste to improve the conductivity. The key goal was to check the efficacy of HPs when the battery cell temperature varies from 20 to 47 °C, and air flowing over the rib structure has a velocity of 2.5 m/s. The results of this research indicate that the temperature of the air flowing over the HP inlet, and the surface temperature of the battery cells have a significant impact on the HP's ability to cool. Using a thermal radiator with ribs in the experimental setup creates more thermal resistance; hence, a better radiator structure is to be selected for high thermal efficiency.

The HP cooling efficiency was defined by the following Eq. 23 [122] as:

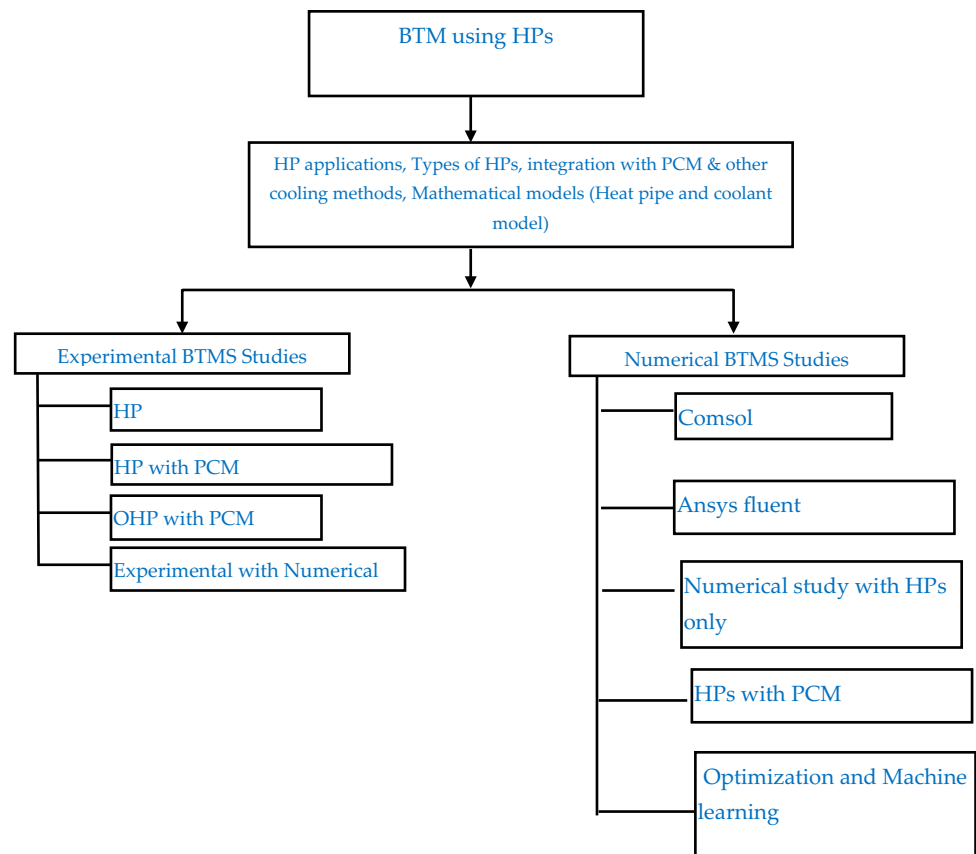
$$\frac{Q_p}{\Delta T_i} = \frac{Q_p}{T_s - T_{in}} \quad (23)$$

where Q_p is heat power, ΔT_i is a difference in temperature at the inlet, T_s is a surface temperature average, and T_{in} is an inlet air temperature.

The thermosiphon HP's thermal conduction at the vapor–liquid junction was given by Eq. 24 [123].

$$q_{tc} = \frac{\beta^2}{\sqrt{2\pi}} \left(\frac{Z}{D} \right)^{\frac{3}{2}} A_s \frac{P_v}{T_{sat}^{\frac{5}{2}}} \quad (24)$$

Fig. 9 The review outline for the present study



where q_{tc} is thermal conduction, β is the latent heat of vaporization, Z is gas molar mass, D is gas constant, A_s is surface area, P_v is vapor pressure, and T_{sat} is saturation temperature.

Hong et al. [124] performed an experimental study on thin-walled ultra-looped heat pipes (ULHPs) used in thermal management power batteries. The study's objective was to check the performance of these wickless evaporator HPs in controlling the battery temperature. The main focus was to determine the most suitable condensation condition for the ULHP with a heat load in the range of 20–80 W. Also, more priority was given to the HT performance of ULHP under the best condensation conditions. The test outcomes found here showed that the startup temperature, startup heat flux, and thermal resistance are minimum for ULHP compared to the conventional loop heat pipes (LHPs) method.

The most common model used to account for heat generation in the battery system was the Bernardi model, represented by Eq. 25 [125].

$$H_g = \frac{1}{V_{bat}} \left(C^2 R_o - C \cdot T_{th} \frac{dA_b}{dT_{th}} \right) \quad (25)$$

where H_g represents heat generation in battery, V_{bat} is battery volume, C is charge/discharge current, R_o is ohmic

resistance, T_{th} thermodynamic temperature, and $\frac{dA_b}{dT_{th}}$ is temperature influence coefficient.

Zhao et al. [126] demonstrated the usage of HPs along with the wet cooling method in a Li-ion battery pack as a thermal BMS experimentally. The main objectives of this study were to limit the upsurge in battery pack temperature and reduce the temperature gradient. Various combinations and arrangements of heat pipes were used in this study, such as heat pipes in natural cooling, heat pipes in forced cooling with a horizontal and vertical position of the fan, and heat pipe with a thermostat bath. The outcomes achieved from this investigation depict that the usage of HP under natural convection was not suitable at a high discharge rate due to more heat production; HPs with water bath was also not recommended for cooling due to the formation of bubbles in the heat pipe, which may act as a resistance to heat transfer; finally, the mixture of HPs with wet cooling methods shows to be a good method in reducing and controlling the battery temperature under various discharging rate. In an experimental investigation, Liu et al. [127] investigated the use of 3-D ultrathin micro heat pipes (UMHPs) to cool a Li-ion battery pack made up of prismatic cells. For the purposes of analysis, the segmented, non-segmented, and thermal network models of HP thermal resistance were used

in this study. The main objective of this investigation was to assess the peak rise in battery pack temperature, difference in temperature between individual cells, and peak temperature variation within the pack. The outcomes of the study predicted that the usage of UMHP gives a very compact design for the BTMS and can control the battery pack temperature. Using natural cooling without HP was inefficient in mitigating the temperature. An experiment was conducted by Deng et al. [128] to examine the effectiveness of HP with fins (HPWF) on BTMS. The test was conducted under different discharge rates, such as 50, 75, and 100 A. The results are compared between the HPWF and heat pipe without fins and natural convection. The usage of HPWF better governs the maximum pack temperature compared to the other two methods. At an ambient temperature of 37 °C, the battery temperature is found to be unaffected by the state of charge (SOC).

Jouhara et al. [129] conducted an experiment to examine the effectiveness of flat mat-type HPs in cooling lithium-titanate prismatic batteries consisting of sixteen cells. The study successfully demonstrated that utilizing HPs as a mat can effectively regulate the battery cell temperature within the optimal range by removing heat from the cells and transferring it to coolants such as water or refrigerant. By using this method, a temperature uniformity of ± 1 °C and a peak temperature of 28 °C for the battery pack were both maintained. The utilization of heat mats could significantly enhance the performance and lifespan of batteries. In a study carried out by Feng et al. [130], the thermal and strain levels of cylindrical cell Li-ion battery packs under atmospheric and forced convection flow with embedded HP were investigated. The study concluded that using a HP cooling device with the forced convection method was a more effective way to regulate the temperature and strain rate within the battery system. The components used for experimental work are subjected to an uncertainty test performed using the Schultz and Cole method given by Eq. (26) [130].

$$E_r = \sum_{i=1}^n \left(\frac{\partial R}{\partial E_i} E_{vi} \right)^{2/2} \quad (26)$$

where E_r is the total error, and E_{vi} is an error of each parameter.

Smith et al. [131] carried out the heat transfer (HT) investigation of prismatic battery cells with a heat load capacity of 400 Watts cooled by using heat pipe plates experimentally. It is observed that using a two-phase heat pipe flow controls, the uniformity in temperature among battery cells very effectively compared to the conventional cooling method. It is concluded from the obtained results that the usage of HPs having water as a coolant having intake temperature of 25 °C, and 1 Lmin⁻¹ discharge is

better in controlling and keeping the battery cell temperature within a limit of 55 °C. Ye et al. [132] experimentally performed a study on rectangular LIB cells organized in series and subjected to free and artificial convection with a micro heat pipes array (MHPA) device. The temperature of the battery pack and the temperature variation between the Li-ion cells are monitored while the battery is being charged and discharged. The use of MHPA with a forced convection environment drastically advances the battery pack's life and durability. Apart from this, the proposed cooling method of MHPA gives high energy efficiency (Eq. 27), ease to manufacture, and compactness.

$$\alpha = \frac{\epsilon_c - \epsilon}{\omega} \cdot 100\% \quad (27)$$

where α is the coefficient of energy conversion, ϵ_c sum of charge and discharge energy in cycle with cooling, ϵ charge discharge energy sum without cooling, and ω is the energy dissipation of the fan. High-temperature regions are observed for a cooling system without MHPA, while better control over temperature distribution can be achieved by using the MHPA system. Ariantara [133] experimentally carried out a study on a prismatic LIB simulator with the usage of loop heat pipes (LHPs) having lotus-type porous (LTP) copper wick for regulating the temperature upsurge in battery system. The proposed method of LHP in a BTMS keeps the battery temperature below 50 °C when heat production is around 20 Watts, while the mean temperature of the system can bring down from 93 to 55 °C by using LHP with LTP wick.

Worwood [134] conducted a study on cylindrical LIB cells to investigate methods for improving the internal thermal management and reducing the temperature rise during high thermal loads. Two models of cylindrical battery cells were employed to analyze the impact of internal cooling on thermal performance. The study found that implementing an internal cooling method can significantly improve thermal management, resulting in a reduction of up to 68% in temperature rise and an increase in the battery system's total performance. These findings have potential implications for the design and optimization of battery systems in various applications.

For an effective operation of HP, the capillary pressure is determined by using Eq. 28 [135]:

$$P_c = P_1 + P_v + P_g \quad (28)$$

where, P_c = Pumping pressure in capillary. P_1 = Drop in liquid pressure in porous wick. P_v = Drop in Vapor pressure from evaporator to condenser. P_g = Gravitational Pressure head.

The pumping pressure by capillary action is given by Eq. 29 [135]:

$$P_c = \frac{2\sigma\cos\alpha}{Rc} \quad (29)$$

where σ —surface tension, α —wetting angle, and Rc —radius of the pore.

Liang et al. [122] performed an empirical investigation to suggest the best possible method for a BTMS using HPs. The aim was to control the battery temperature and its uniformity by regulating the fluid temperature used in the HP. The thermal efficiency of the BTMS was examined in relation to the effects of fluid temperature, air temperature, and fluid flow rate. The study found that implementing an intermittent cooling strategy can significantly decrease power consumption in the battery system. The impact of power input, coolant flow rate, and ambient temperature on the peak battery temperature was analyzed. The results clearly showed that the coolant discharge and surrounding temperature are crucial factors in regulating the peak battery temperature. Gan et al. [136] experimented on a cylindrical battery pack of cells that was cooled naturally and with heat pipes, and the results were promising. The parameters like the discharge rate of batteries and fluid, and intake fluid temperature are studied to determine battery cell temperature characteristics. In this research, a thermal equivalent circuit model (TECM) was put forth to assess the thermal behavior of the battery pack. It was noted that by using HPs for BTMS can reduce battery cell temperature to a greater extent up to 14 °C for 5 °C discharge rate. The arrangement of BTMS was seen to be crucial in this study. The HPs are inserted between the battery cells, and the condenser unit of the HP is situated in the cooling channel.

Equation 30 [136] is used to describe how much heat is produced within the battery cell

$$H_{bc} = D_c^2 R_i \quad (30)$$

where H_{bc} is heat is generated inside the pack, D_c is current discharged, and R_i internal thermal resistance. When high discharge rates are used for battery, the entropic heat is neglected as compared to Joule heat.

Zuo et al. [137] proposed an integrated BTMS that uses HP cooling and preheating with a heat pump AC system. Experiments were conducted for different arrangements, and a viable solution to the battery cooling issue was discovered by implementing an additional chiller without increasing the power consumption. The influence of gravity makes heat pipes perform better in preheating mode conditions rather than in cooling mode. The integrated BTMS preheating and cooling system coupled with the heat pipe system was shown. This study provided good performance of HPs in transferring heat from the battery cabinet. The effectiveness of the micro HPS array (MHPA) for cooling the rectangular battery cells was experimentally examined by Xin Ye et al. [138]. The test was conducted for different charging and

discharging rates, and it is found that for 1C and 2C charge rates the thermal performance of the battery has improved a lot. This study aims to address the safety and durability concerns of battery modules under varying operational conditions. The configuration of the MHPA involves placing the evaporator section of the HP between the battery cells, while the condenser section is exposed to the ambient environment, multi number of channels were made in the HP, and each channel has a number of inbuilt fins. The heating of battery cells by both traditional methods as well as by MHPA method. The temperature of the battery reduces more noticeably using the new method than it does using the conventional heating technique in the same amount of heating time. To prevent the thermal runaway of the batteries, Putra et al. [139] conducted an experimental analysis of rectangular LIB cells cooled by flat plate loop heat pipes (FPLHPs). Three different coolants, like distilled water, acetone and alcohol, are used with 50–80% filling, while the battery is subjected to three different heat loads. Battery heat generation is simulated by making use of a cartridge heater. Among three different coolants, acetone is found to give excellent performance in regulating BTMS temperature. In the current investigation, the FPLHP heat-exchanging device was utilized. It mainly consists of evaporator, condenser, heater, and flat plate. The flat plate is held between the heater and the evaporator part. The flat plate conducts the heat, and from the flat plate, it is taken away by the evaporator section, from the evaporator to the condenser. The summary of the experimental works using HP for BTMS is presented in Table 2 below.

Experimental BTMS analyses using heat pipes (HPs) coupled with PCM

Putra et al. [140] carried out an experimental study to investigate the usage of HPs with PCM for the passive cooling of rectangular Li-ion batteries. The PCM used in this study was beeswax, and experiments were conducted in both the presence and absence of HPs and beeswax. Transient examination was performed to assess the thermal behavior of the batteries, and a comparison was made between the use of beeswax PCM and Rubitherm RT44. The results obtained demonstrated that the usage of beeswax PCM in HPs decreased the temperature by up to 26.62 °C, while the usage of RT44 in HPs reduced the temperature by 33.42 °C. A prismatic LIB cell with a coupled cooling strategy involving a heat pipe and a PCM was experimentally analyzed by Jiang and Qu [141]. A wide range of parameters has been experimentally studied, such as the battery charge and discharge cycle, convection coefficient, the surrounding temperature, and PCM thickness ratio of the battery. The outcome suggested that the MP of the PCM must be minimum 3 °C more

Table 2 Summary of experimental works using HP for BTMS

Battery geometry	Input parameters	Analyzed parameter	Coolant used with heat pipe	Remarks	Reference
Cylindrical	Discharge rates, Discharge Current, Distance from Center of battery in radial and axial direction. Cut off Voltage 2.8 V	Battery Surface Temperature	Liquid	Heat production in battery, thermal conductivity, density, heat capacity were assumed to be uniform, electrolyte motion was neglected, and radiation effects were neglected. When the discharge current reaches a value of 10A, the temperature at the battery surface reaches to 65 °C	[116]
Prismatic	Input power to battery, Heating time	Maximum battery temperature, Temperature difference	Water	Power input of 30W with heat pipe and heating time of 400 to 600 s gives the best efficient results in terms of temperature rise and temperature difference	[117]
Cylindrical	Position of heat pipes such as horizontal, vertical and inclined (10°, 20°), power of the battery, air velocities	Maximum temperature, Temperature gradient, stabilization time, Thermal resistance	Water	Compared to the heat sink, flat HPs are more effective in controlling the temperature uniformity inside the battery cells and suitable for any type of road HEV uses	[119]
Prismatic	Input power to battery cell, discharge rate of battery, heating and cooling time	Surface temperature of battery cell, Average temperature drop in the cells, Performance of battery with and without heat pipes	Glycol–water	When the power input for each battery cell was increased up to 20 or 30 W, the battery cell temperature may reach the value of 100 °C and at this temperature, the battery performance deteriorates. Usage of heat pipes at such high input power brings down the temperature in between 60 to 70 °C	[120]
Prismatic	Transverse and longitudinal thermal conductivity of the cell, surface temperature, air inlet temperature, air velocity	Peak temperature of battery cell, temperature variance, heat pipe cooling efficiency	Liquid Butane	The inner wall of HP is covered with two-dimensional mesh to improve the cooling efficacy of the HPs. The vapor velocity within the heat pipe decreases hence does not have much effect on pressure drop	[121]
Prismatic	Different condensation conditions, heat load, fan voltage, heat flux, Charging/Discharging current	Battery temperature, Thermal resistance, Pressure	Water	ULHP can operate effectively under different range of heat load from 20 to 120W, the ULHP used have low startup temperature with voltage input of 9 V to fan and thermal contact resistance of 0.097 K/W, ULHP also operate effectively under charge and discharge value of 2.5C	[124]

Table 2 (continued)

Battery geometry	Input parameters	Analyzed parameter	Coolant used with heat pipe	Remarks	Reference
Prismatic battery pouch	Battery Capacity (3Ah and 8 Ah), Different charge rate, Fan position (Vertical and Horizontal)	Temperature rises in battery, Temperature gradient,	Acetone	Heat pipes and wet cooling control the temperature rise in 3Ah battery pouch within 4 °C. Temperature difference across the cells is hardly about 1.5 °C. The 8Ah battery pouch can be kept at a temperature of under 30 °C for various discharge rates	[126]
Prismatic	Different discharge rate,	Max temperature rise, max temperature gradient in battery pack and cells	Water	The dynamic thermal characteristics of EV batteries is performed and the following results were stated. The air convection combination with UMHP proves to be moderate in reducing the maximum temperature, UMHP with natural convection have the least effect on maximum temperature, while the forced convection UMHP is more effective to control instant heat generation	[127]
Prismatic	Different discharge rate, state of charge, Pulse cycling process, discharge depth	Rise in maximum battery temperature and its uniformity	Water	The findings indicate that as velocity increases, the battery surface temperature rises, and temperature consistency declines. The battery pack temperature upsurge varies with the depth of discharge and pulse cycle rate. The constant discharge rate does not make much difference in the battery temperature for both the case (HPWF and HP)	[128]
Prismatic battery cell	Maximum temperature, temperature variation along length, height and width of the cell, state of charge, DC power	Peak temperature, Temperature homogeneity	Water and Refrigerant	The Peak temperature limit for the cell is around 55 °C, and the temperature homogeneity of the battery pack relies on cell height, length, and width	[129]
Cylindrical battery cell	Maximum temperature, strain value, Different discharge and charge rate, forced, natural convection	Maximum temperature limit and strain value limit		In order to regulate the temperature, the battery pack does not use natural convection cooling. The strain rate and battery pack temperature upsurges with a rise in fluid velocity.	[130]
				Best method to depress the strain and temperature with compact size	

Table 2 (continued)

Battery geometry	Input parameters	Analyzed parameter	Coolant used with heat pipe	Remarks	Reference
Prismatic Battery cell	Maximum Temperature, Heat load, Thermal resistance	Temperature distribution in cooling plates, condenser, evaporator, and separator	Water	The proposed BTMS using heat pipe cooling plates is a better choice in controlling the battery pack module temperature of 55 °C, at a heat load of 400 Watts. Better temperature uniformity is obtained among the cells of the battery with a range of ± 5 °C	[131]
Rectangular battery cells	Charge and discharge rate, power input to the battery pack, natural and forced convection	Temperature variance among the cell and battery pack, Temperature uniformity	Water	By the application of MHPA device, the temperature variance among the cells and battery pack is kept under 5 °C. Using MHPA with fins under forced convection increases the rate at which heat is drained away from the battery pack	[132]
Prismatic Battery Pack	Rate of heat production of 20 W, 30 W and 40 W	Battery surface temperature, Battery thermal resistance	Cold water	The results indicated that using LHP and LTP wicks the battery pack simulator temperature with different heat generation rates can be kept within the permissible and safe limit	[133]
Cylindrical battery cells	State of charge (SOC), Heat transfer coefficient, Thermal Conductivity, and single- and double-tab cooling	Internal Thermal Resistance, Cell heat generation, cell current, Maximum cell temperature, Pumping power	Water	For better internal battery cell thermal management, an external cooling system is needed. To achieve an efficient heat transfer rate, reducing the internal thermal resistance of the battery cell is a necessary step	[134]
Prismatic battery cell	Coolant velocity, surrounding temperature, heat generation rate	Maximum cell temperature, temperature difference between the cells, pumping power consumption	Sintered copper water	By enhancing the coolant velocity and reducing the coolant ambient temperature, the efficacy of HP-BTMS can be enhanced to a greater extent. The thermal performance can remain unchanged when the ambient temperature is kept below 35 °C	[122]
Cylindrical cells	Coolant intake temperature, coolant discharge rate	Battery cell temperature	Sintered copper water	It is concluded that the HP BTMS implementation may result in a decrease in the battery cell's temperature	[136]

Table 2 (continued)

Battery geometry	Input parameters	Analyzed parameter	Coolant used with heat pipe	Remarks	Reference
Prismatic battery cells	Coolant temperature, Preheating mode	Heat transfer performance, Battery cell temperature	Water ethylene glycol	The use of an additional cooling chiller in the battery system increases the cooling capacity by 20% without increasing the input power. The integrated method of cooling and the utilization of preheating has demonstrated to be effective in managing the increase in battery temperature	[137]
Rectangular battery cells	Charge-discharge rate, heating time, heat production rate	Battery Temperature both in cooling and heating, Temperature difference	Water	With the usage of MHPA the battery module temperature is controlled under 32 °C and 39 °C, with the charge-discharge rate of 1 C and 2 C	[138]
Prismatic battery cells	Coolants, Heat flux	Temperature of battery module	Distilled Water, Alcohol, Acetone	The use of Acetone in the evaporator section can keep the battery's temperature around 50 °C, at heat flux 1.61 W/cm ² , with a thermal resistance of 0.22W/°C	[139]

compared to the surrounding temperature for effective cooling effects and less power consumption. At the condenser unit of the HP, a convective coefficient of 30 to 60 W/m²K is sufficient, while the thickness ratio of PCM is around 0.55. The variation in battery module temperature with HP/PCM cooling strategy and the surrounding ambient temperature are elucidated. It is observed that with a temperature span of 35 to 40 °C the battery module HT is only through HP, as the PCM material will not melt at this temperature range. Experiments on a prismatic LIB module with heat pipes and a PCM cooling technique were done by Wu et al. [97]. Different discharging cycles and forced convection coefficients were chosen as input parameters. It was seen that at a greater discharge rate of 5C, it is possible to maintain the temperature of the battery module at 50 °C. The use of PCM along with HPs can reduce power consumption by cooling the fan at a lower flow rate. The experimental setup for the battery module thermal cooling system is shown. It consists of a HP sandwiched between the blocks of PCM; the heat from the batteries is transported to HPs via PCM and rejected at the HPs condenser unit, which has fins at its outer surface. The variation in battery temperature across the module with a change in discharge rate is shown. Three cooling modules are used for cooling without PCM, with PCM and with HP and PCM. With an upsurge in the velocity, there is a noticeable rise in the peak temperature difference in the battery module but less increment is observed in the case of PCMP and HP/PCM.

In order to examine the thermal performance of Li-ion cylindrical batteries with various cooling systems, Zhao et al. [103] performed an experiment. Air cooling, a PCM without HPs, and a coupled HP and PCM system (HP/PCM) were the cooling methods employed in this study. The findings demonstrate that the HP/PCM combination outperforms the air-cooled BTMS in terms of maintaining the battery temperature within 50 °C for a longer period of time. Additionally, the battery module's peak temperature difference could be kept to below 5 °C for an extended period of time. Zhang et al. [142] suggested different cooling strategies based on separation BTMS assisted by heat pipes. The different discharge rate of the battery is used along with discharging cycle. The experiments are conducted under forced and free convection conditions. The obtained results show that using PCM and HP cooling method; the battery module temperature can be regulated very effectively and provides some useful design parameters for optimization of BTMS. The BTMS for prismatic LIB cells was studied by Amin et al. [143] under three cooling conditions: cooling without HP/PCM, cooling with HP, and cooling with HP/PCM. The input heat load to the battery cell is varied from 20 to 50W. The results of this experimental investigation show that using an HP/PCM combination is appropriate for keeping the battery temperature below 50 °C. By utilizing HPs,

PCM, and spray cooling, Lei et al. [144] provided an experimental design for the heating and cooling of prismatic Li-ion batteries. The battery performance is analyzed at a different surrounding temperature varying from $-10\text{ }^{\circ}\text{C}$ to $40\text{ }^{\circ}\text{C}$. The heating service by the proposed method can diminish the chances of battery degradation. The proposed method also demonstrates improved cooling performance by effectively regulating the battery surface temperature despite at a high discharge current rate of 24A and an ambient temperature of $40\text{ }^{\circ}\text{C}$. Huang et al. [145] conducted experiments to examine different cooling strategies for cylindrical LIB modules including HPs with air-aided PCM and HPs with liquid-aided PCM. They varied the discharge rate of the battery to analyze the temperature behavior of the battery module. According to the study's findings, HPs with liquid-assisted PCM can efficiently maintain battery temperatures below $50\text{ }^{\circ}\text{C}$ at a 3 C discharge rate. Table 3 summarizes the results of the work using HP/PCM combination.

Numerical BTMS analyses using heat pipes

Zhao et al. [146] analyzed the prismatic battery module of Li-ion fixed with closed loop OHP (CLOHP) and PCM. The input heat load on the battery varies from 10 to 80 W with various coolant discharge rate and the number of turns. While CLOHP's number of turns significantly impacts thermal performance, using it with PCM improves it. Finally, it is also concluded that it is challenging to maintain the liquid–solid state of PCM at higher heat input loads. OHP's cooling performance for high energy density Li-ion batteries was experimentally investigated by Chi and Rhi [147]. Different configurations are used for OHP in order to check the HT characteristics. The Li-ion battery is modeled as a heater with a required heat generation rate, and parameters like filling ratio, coolant temperature, the orientation of the HP, and heat flux are analyzed experimentally. This study's outcomes suggest that the usage of the OHP cooling system meets the required BTMS design parameters. A similar type of experimental study on OHP is done by Rao et al. [148] in which a rectangular heater made up of an aluminum block is used as a simulator for the actual battery model. Different heat load on the heater block and the location of OHP is used as input to examine the thermal efficacy of BTMS. The battery terminal's location and OHP orientation have an important part in governing the temperature rise in the batteries. Wang et al. [149] examined OHP/PCM-based BTMS. The input variables used in this study are heat load on the battery and battery terminals' position of OHP. It is better to keep the temperature and difference in temperature below the PCM melting point to have uniform temperature distribution. The use of PCM with OHP gives a very effective cooling of BTMS as compared to only OHP.

Wei et al. [150] examined an plug-in OHP to provide better and more effective cooling in BTMS. An equivalent electric heater just simulating the Li-ion batteries is used. The findings led to the conclusion that a 56W power input can keep the battery temperature below $46.5\text{ }^{\circ}\text{C}$. They also noticed that it is possible to effectively maintain the peak temperature variance within the battery module at $1\text{--}2\text{ }^{\circ}\text{C}$. With plug-in OHP, the uniformity in battery temperature can be maintained very smoothly. It can be clearly observed that at a binary fluid mixture ratio of 4:1, the temperature in the OHP rises with a rise in the power input. However, the difference by which temperature increases decreases with power input. Table 4 provides a summary of an experimental analysis of BTMS using oscillating heat pipes coupled with PCM.

Numerical BTMS analyses using heat pipes

Dan et al. [151] examined a system consisting of micro HP array (MHPA) to manage the system thermally in electric vehicles. The system consists of 96 similar batteries with MHPA sandwiched between two batteries with condensation facilities at the ends. Dan et al. [151] numerically examined prismatic LIB cells cooled by a MHPA inserted in between the battery cells under forced convection conditions. The numerical results are validated with actual results under steady and dynamic conditions. Both MHPA- and single-battery forced convection are computed, and the temperature upsurge and gradient of the battery module are compared. They used the AMESim environment to perform numerical modelling and simulations on the equivalent thermal resistant model of the MHPA. The results were obtained regarding heat transfer efficiency during constant discharge, temperature distribution during transient operation, and cooling effects on large battery packs. The obtained results were validated with the experimental results. They concluded that temperature is the critical factor that affects the battery's serviceability, discharge efficiency, and power. They also delineated that reducing the operating temperature can enhance battery performance. Moreover, the results obtained from simulations of the cooling of batteries concluded that there is an insufficiency of natural convection to cool the batteries at a significantly high discharge rate.

The effects of using HPs and copper tubes on the TM of high-power lithium batteries were compared by Wan [152]. He prepared the simplified model by considering the transient characteristics as linear differential equations using assumptions and avoiding the battery's electrochemical reactions to reduce the computational time. The heat pipe model formulation consists of a copper shell, wick region, and vapor core. The thermal conductivity, density, and heat

Table 3 Overview of experimental and numerical analysis of BTMS using HP/ PCM combination

Battery geometry	Input parameters	Analyzed parameter	Coolant used with heat pipe	PCM material	Remarks	Reference
Rectangular battery	Passive cooling by heat pipes and PCM	Battery temperature	Water	Beeswax and Rubitherm RT 44	The battery thermal performance can be improved by using heat pipes, and PCM as a better choice for cooling the Li-ion batteries	[140]
Prismatic battery module	Charging and discharging cycle, PCM and battery thickness ratio, ambient temperature, convective heat transfer coefficient	Battery temperature	Water	PCM+expanded graphite	The combination of the HP/PCM can regulate the long run of the battery system. Less power consumption, long battery life, and safety can be guaranteed with HP/PCM cooling strategy	[141]
Prismatic battery module	Discharge rate, forced convective coefficient	Peak temperature of battery, Temperature variance in battery module	Sintered copper Water	Paraffin and expanded graphite	The usage of PCM with HPs is the best feasible BTMS technique for EV's and HEV's. In the battery module, temperature uniformity is obtained by using PCM	[97]
Cylindrical Cell	Discharge rate, air velocity, input power	Peak temperature, Temperature difference	Water	Paraffin/EG	Using an HP can speed up the phase transition of PCM materials and increase temperature uniformity	[103]
Prismatic battery cell	Discharge rate, cooling modes, Discharge cycle	Peak temperature, minimum temperature and temperature difference	Deionized water	Paraffin composites	For a discharge rate of 5C or higher, the battery temperature may exceed 45 °C. The HP PCM usage with forced convection avoids the temperature imbalance among the cells	[142]
Prismatic battery cell	Cooling methods, Heat load on the battery	Maximum Temperature	Water	Beeswax	HPs can reduce the temperature of the battery's surface by 7.1 °C, while the combination of HP+PCM reduces it by 10 °C	[143]
Prismatic battery cell	Room temperature, Discharging current in amperes	Maximum surface temperature, temperature difference, average battery surface temperature	water	Hydrated salt	The proposed heating and cooling strategy for BTMS increases the electric energy output from 39.5 to 62.5% Even at high discharging rates, 2.6 °C can suppress the peak temperature difference in a battery cell	[144]

Table 3 (continued)

Battery geometry	Input parameters	Analyzed parameter	Coolant used with heat pipe	PCM material	Remarks	Reference
Cylindrical batteries	Discharge rate, Cooling methods	Maximum temperature, temperature difference	Water	Mixture of paraffin and graphite	In combination with liquid-assisted PCM, heat pipes are a better choice for controlling the battery temperature within 44 °C for an extended time run. The temperature difference between batteries can be limited to 3 °C, maximum	[145]

capacity of the wick region is obtained using the equations represented below [152]:

$$k_{\text{wick}} = \frac{k_1 [(k_1 + k_s) - (1 - \varepsilon)(k_1 - k_s)]}{[(k_1 + k_s) + (1 - \varepsilon)(k_1 - k_s)]} \quad (31)$$

$$\rho_{\text{wick}} = \varepsilon \rho_1 + (1 - \varepsilon) \rho_s \quad (32)$$

$$C_{\text{wick}} = \frac{[\varepsilon \rho_1 C_1 + (1 - \varepsilon) \rho_s C_s]}{\rho_{\text{wick}}} \quad (33)$$

where k_1 and k_s are the thermal conductivities of coolant and sintered copper powder, and ε is the porosity.

Using commercial finite volume-based Ansys Fluent 17.2 software, Wan [153] carried out the numerical simulation on a battery cell. The PDEs were solved by taking a staggered grid. The pressure was solved using SIMPLE algorithm. Real time boundary conditions were imposed to solve these partial differential equations. The coolant intake temperature, discharge and power load on the battery are the parameters selected for the simulation purpose. The usage of HPs and copper rods for cooling are compared. From the results obtained, it is clearly observed that HPs can enhance the HT from the battery cell compared to copper rods. This numerical study also demonstrates the surface temperature and heat flux distribution in the battery cells. The density of wick material having porosity with copper sintered and liquid water filled is obtained by using the below Eq. (34) [153]:

$$\delta_w = \varepsilon \delta_1 + (1 - \varepsilon) \delta_c \quad (34)$$

where δ_w is the wick density, δ_1 liquid density, δ_c sintered copper density, and ε porosity of the wick. According to the study, there is a direct relationship between the peak temperature inside the battery cell and the temperature of the coolant inlet and power input, with an increase in either of these factors causes a rise in temperature. However, as flow rates go up, the battery's peak temperature decreases.

In order to reduce computation time and expense while maintaining acceptable accuracy, Liang et al. [154] designed a 3D battery thermal model and took flow decoupling and conjugate heat transfer (CHT) analysis into account. They did this by segmenting the battery module into sub-models for CHT, heat pipe, and multi-cells. They found a reduction in temperature of the battery cells. A numerical conjugate assessment of a Li-ion battery module connected in series and cooled by HPs was carried out by Yunhua Gan et al. [155]. To investigate the dynamic temperature, current density, voltage, and Li-ion concentration, the coolant inlet temperature and flow velocity are varied. According to the results, a peak temperature is seen in the battery cell's first module at low coolant

Table 4 Summary of the experimental analysis of BTMS using oscillating heat pipes coupled with PCM

Battery geometry	Input parameters	Analyzed parameter	Coolant used with heat pipe	PCM integrated material	Remarks	Reference
Prismatic battery	Heat load, flow rate of liquid coolant, number of turns in CLOHP	Battery temperature, thermal resistance	Deionized water	Paraffin wax	The oscillation stability of CLOHP depends on the number of turns	[146]
Prismatic battery	Heat input, coolant temperature, heat flux, and orientation of OHP	Temperature, power spectrum density, Thermal contact resistance	Methanol	No	The coolant filling rate of the used in OHP is a crucial issue that influences its HT performance. Along with the orientation angle	[147]
Prismatic batteries	Heat input, OHP orientation	Temperature, Temperature difference	Acetone	No	The vertical positioning of the OHP is found to be better than the horizontal positioning for regulating the temperature rise in both battery and OHP, for the given input parameters	[148]
Prismatic Battery	Heat input, surrogated battery terminals, and OHP position	Temperature, Temperature difference, Temperature uniformity	Acetone	Paraffin	To reduce the aggregate battery system temperature, it is more effective to utilize a lower start-up temperature for the OHP as compared to the PCM. It is good to locate the battery terminals away from the OHP adiabatic unit	[149]
Prismatic battery module	Heat input, Binary fluid mixture ratio, filling ratio	Temperature, temperature difference	Ethanol, and Water	No	The mixture of ethanol and water shows excellent heat transfer performance as a working fluid in OHP compared to pure water or ethanol	[150]

temperatures, and the Li-ion concentration is significantly affected at the battery cathode side. The thermal performance of the HP is defined by incorporating the HP sub-model in CHT. They used COMSOL 5.3 to carry out the simulations. The tool based on FEM was used to solve the PDEs. The spatial domain was divided into a number of simple geometries (quadrilaterals). The solution function for each domain of finite elements is then approximated using the weighted residual idea. The dependent variables and their first partials were maintained when shifting from one element to another. This results in the transformation of PDEs into sets of ODEs over time. Using 2nd central differencing scheme, the equations are discretized. The sub-models were validated, and moreover, the whole battery was also validated through experimentation. They thoroughly investigated the thermal as well as the electrochemical performance of the three-dimensional model for different temperature conditions of coolant. They observed that the lithium-ion concentration and local current density change at the same rate during the initial discharge phase, and huge local current density also exists. Moreover, significant effect of cooling temperature on the positive electrode with respect to negative electrode. Furthermore, they observed that when the coolant temperature is decreased by 10 °C during discharge at 5C, the available capacity of the battery is reduced by 0.88–1.17%. It is very difficult to get the 3-D simulation of the whole battery system, including the thermal electrochemical process; hence, to simplify the model, a number of sub-models are created, such as CHT sub-model, heat pipe sub-model, and multi-cell sub-model.

Wang et al. [156] examined a HP-based TMS for the battery module, which consists of four rows of cylindrical batteries in the x direction, with each row having three batteries sandwiched between the three HPs with aluminum as a conduction element. Moreover, Wang described that there are several factors that influence the battery module's temperature distribution, namely (a) spacing between batteries (D), (b) thickness (δ), (c) height (H), and battery circumferential angle (θ). To determine and analyze the effect of the influential factors mentioned above on BTMS, CFD analysis is done using finite volume based ANSYS Fluent 17.0. Equations are discretized using the finite volume method (FVM) by means of a 2nd order central differencing scheme. By solving the associated continuity and momentum equations using the SIMPLE method, the velocity and pressure components are obtained. Coupled energy and conduction are also solved simultaneously since heat flow and temperature at the contact are continuous. The ensuing algebraic equations are numerically addressed using successive over relaxation, the tridiagonal matrix method, and line-by-line Gauss–Seidel. The following governing equations are used for the module.

The energy conservation equation is represented as [156]

$$\rho_b C_{pb} \frac{\partial T}{\partial \tau} = \nabla \cdot (\lambda_b \nabla T) + \dot{Q} \quad (35)$$

with \dot{Q} as the source term given by the rate of heat production and battery volume represented as Q_{gen} and V_b .

$$\dot{Q} = \frac{Q_{\text{gen}}}{V_b} \quad (36)$$

Moreover, a grid sensitivity test of the mesh shown is done to guarantee the calculation accuracy. Moreover, they validated the numerical model with the experimental ones. After performing the tests, they came to the conclusion that the height of the element is the most sensitive element affecting the peak temperature of the battery module after conducting the tests. The other factors like circumference angle, spacing between batteries, and thickness have minimal effect. Moreover, after doing the sensitivity analysis, they prepared an optimal model with conduction element height (60 mm), circumference angle (120°), conduction element thickness (4 mm), and spacing between batteries (19 mm), respectively. They performed the numerical simulation on the battery and observed a minimum temperature difference (1.08 °C) and a maximum temperature (27.62 °C). The obtained values for the optimal design of the structure are 4 mm conduction element thickness; optimal spacing should be 19 mm and the circumferential angle should be 120°. The optimal model suggested in this study provides the best thermal management system compared to other models.

By regulating the core temperature in the battery pack, Huang et al. [157] conducted a numerical analysis on Li-ion batteries employed in HEVs to increase the battery life and durability. Different mathematical models' controller is used to predict the battery temperature while minimizing power consumption. The battery's core temperature can be kept well below the limit with only a small amount of power consumption, according to the cooling models used in this study. Each module consists of 10 cells. A flat plate heat collector takes the battery module heat and transfers it to the surrounding ambient air through a HP. The chains of numerical simulations were performed using MATLAB/Simulink considering different operating and ambient conditions to assess the battery's thermal performance. They used a four-wheel HEV, which consists of an IC engine, hub e-motor, and 14 battery modules constructed using MATLAB/Simulink. These battery modules are based on HPs cooling systems. The simulation is performed for three different ambient conditions for each driving. The results show that UA with an 10 °C surrounding temperature is capable of maintaining battery core temperature with the tracking error of 0.8 °C. Moreover, they also investigated cooling system adaptiveness under the ambient temperature of 25° and found that the first mode only functions well when the temperature of the battery remains

below the higher level. For the ambient temperature of 40 °C in CE driving cycles and third mode, the compressor compensates the increment in thermal load. After carefully analyzing these results, they came to the conclusion that the suggested solution might maintain the battery core's temperature within the desired range since the ambient air cooling is sufficient for the first mode, for the second and third modes, ambient cooling may fail, so AC pathways are required. It is clearly observed that for Mode-I and Mode-II, the core temperature will oscillate more and remain unstable, while for Mode-III, these oscillating effects can be compensated, and hence, the core temperature remains within the maximum limit.

The mathematical modeling of the thermal runaway of series-connected prismatic battery cells was carried out by Li et al. [158] using FVM. (A discretization technique for approximating a system of PDEs describing the conservation, or balance, of one or more parameters) The user-defined functions (UDFs) are written to determine the HT between the battery cell and HPs. Thermal runaway propagation from one battery to its adjacent battery is simulated for various working conditions. Three battery cells arranged in series are placed side by side. The condenser unit of the HP is fixed with fins to improve the HT rate. The simulation of the thermal runaway model and the volume of fluid model is done in the ANSYS FLUENT to investigate the transfer of heat and mass within the battery cells, during the thermal runaway. The finite difference approach is used to approximate the derivatives. Following that, the face values for u , v , and P are calculated. For the temporal derivative, a backward difference is used, and for the spatial derivatives, a central difference is used. The equation gives the generation of heat and energy conservation during the thermal runaway [158]:

$$q_{abuse} = H_{sei} W_{sei} \left| \frac{dc_{sei}}{vt} \right| + H_{ne} W_{ne} \left| \frac{dc_{ne}}{dt} \right| + H_{pe} W_{pe} \left| \frac{d\alpha}{dt} \right| + H_e W_e \left| \frac{dc_e}{dt} \right| \tag{37}$$

$$C_p \frac{\partial T}{\partial t} = \nabla \cdot (k_i \nabla T) + q_{abuse} \tag{38}$$

The outcome indicate that the HP-based cooling system is ineffective at preventing the battery's thermal runaway. However, it can stop propagation between batteries that are close to one another. The liquid water absorbs the heat from the battery cell and transforms from a liquid to a vapor as time passes from 1 to 10 s. The temperature profile in each battery as the heat propagates through them was presented. Park et al. [82] enhanced the HP loop, generally utilized for the cooling of li-ion batteries in the high-energy electric lasers (HELs) used in aircraft. Their main objective was to optimize using a deterministic and reliability-based method to lighten the LHP's weight considering

varying heat load. A thermodynamic model and a liquid thin wick model were used in the numerical solution. Three different cases are considered to achieve the optimized design for battery cooling, a constant heat load, a variable heat load without uncertainty, and a variable heat load with uncertainty. Among the three cases investigated in this study, the most reliable and robust one is the case of varying heat load with uncertainty. They also performed the numerical analysis through a thermohydraulic model of the LHP, which comprises of the following elements: compensation space, evaporator, vapor line, and condenser. Moreover, the thin liquid film model is used to forecast HT in the porous wick, and the finite difference method (FDM) and analytical solutions are employed for the thermal characterization of the groove section. The evaporator core and compensation tank energy balance equation is given as [82]:

$$Q_{loss} + Q_{e-c.c} + x_{1,l} \dot{m} h_{fg} = U_{c.c-amb} (T_{c.c} - T_{amb}) L_{c.c} + \dot{m} C_{p,core} (\dot{m} T_{core} - T_{l,l}) \tag{39}$$

They were able to optimize the LHP design while keeping the battery temperature at 10 degrees Celsius and reduce the LHP's weight by 12% when compared to the LHP used by the existing Adonis under identical thermal conditions. They came to the conclusion that the third case, which performed better in terms of success ratio, could be regarded as an excellent contender for the LHP design for military use. It has been noted that the battery temperature changes along with variations in the heat load, but out of three cases, case III gives more reliable and robust results that justify the usage of a loop HP for cooling purposes.

A transient numerical model of the li-ion battery (C020) cell was put forth by Greco et al. [159]. The thermal circuit method, which the one-dimensional, enables separate treatment of the battery and HP. Additionally, a three-dimensional (3-D) model and a quantitative model based on transient boundary conditions were prepared in order to verify the one-dimensional (1-D) model. HPs with working fluid removes heat from the battery cell sandwiched between the set of HPs in series. The study compares the 1-D thermal circuit method, the analytical method, and the 3-D CFD simulation. The results show that the 1-D thermal circuit method is sufficient in predicting the temperature characteristics of battery cells. It is also concluded that the higher contact surface between the HP and the battery cell increases the heat transfer.

The volumetric heat production rate in the battery cell is represented by Eq. 40 [159].

$$Q_v = R_h i^2 - \frac{T \Delta E_i}{mH} \tag{40}$$

where Q_v is volumetric heat production rate, internal heat resistant per unit volume, discharge current per unit volume, m is the number of electron exchanges during discharge, H is faradays constant, and E_i is entropy.

Murashko et al. [160] introduced a thermal protection system that uses metal plates and heat pipes to maintain a uniform temperature in pouch-type cells. They suggested a passive cooling system for the BTMS made of aluminum plates with built-in HPs. Further, they conducted a numerical optimization of the TMS to improve the efficacy and maintain uniformity in temperature distribution. To place the HPs in the aluminum plate in the best possible location, they used COMSOL Multiphysics. The governing differential equation are discretized using a finite element approach. The SST turbulence model with automatic wall function was adopted. The boundary conditions include mass flow rate inlet, pressure outlet, symmetry planes, and adiabatic walls. No-slip condition was set between the liquid and solid. The algorithm used for the optimization was produced in MATLAB. Following optimization, they came to the conclusion that the horizontal portion of the U-shaped HPs should be positioned close to the cell's maximum power loss. Moreover, they also succeeded in reducing the number of HPs without increasing the temperature non-uniformity. Yuan et al. [161] prepared a thermal management module (TMM) that consists of heat pipes of an outer diameter of 6 mm for the primary source of heat transfer along with heat collecting plates and aluminum alloy 6063 cooling fins with a mean spacing of 2 mm between each fin. For the experimentation, they used the lithium iron phosphate battery of 10 Ah capacity as the source of heat. The temperature characteristics of the TMM- fitted batteries were investigated using the testing system in an enclosed and adiabatic environment. They attached the five k type thermocouples to the battery surface at different locations, namely A, B, C, D and E. The temperature variation of each site was tracked at 2.5 °C discharge rate. The five different used locations are sufficient to track the longitudinal variations. Initially, they discussed the thermal issues and the necessity of TMS of li-ion batteries by showing the variation of surface temperature with the discharge rate. They observed that an increased flow velocity is linked to a higher reaction rate, which inevitably leads to an elevated battery temperature. They observed the maximum temperature at point A and the minimum at point E because point A is closest to the electrode tab and E is the farthest. They constructed two prototypes, namely model I (with heat collecting plate) and model II (without heat collecting plate). The temperature transients of model I and model II. After analysis of the plot, they observed the values at the ends of temperature transients of model I exceed the temperature plot of model

II by 6 °C. They concluded that using a heat collector can manage the temperature more efficiently.

Moreover, they validated the experimental results using the CFD model in the commercial software Icepak. After considering certain assumptions regarding thermal parameters and material properties, the heat transfer, temperature field, and boundary conditions are given by [161]

$$\rho C_p \frac{\partial T}{\partial t} = \nabla \cdot (K \nabla T) + q \quad (41)$$

$$\rho C_p \frac{\partial T}{\partial t} = \lambda_x \frac{\partial^2 T}{\partial x^2} + \lambda_y \frac{\partial^2 T}{\partial y^2} + \lambda_z \frac{\partial^2 T}{\partial z^2} + q \quad (42)$$

The initial condition is described by the equation below, where T_0 is the initial value

$$T(x, y, z, 0) = T_0 \quad (43)$$

The other boundary condition in each direction is directed by Newton's law of cooling and is represented as

$$-\lambda_x \frac{\partial T}{\partial x} = \beta(T - T_\infty), x = 0, l \quad (44)$$

$$-\lambda_y \frac{\partial T}{\partial y} = \beta(T - T_\infty), y = 0, b \quad (45)$$

$$-\lambda_z \frac{\partial T}{\partial z} = \beta(T - T_\infty), z = 0, h \quad (46)$$

The parameter β represents the HTC, T_∞ —ambient temperature and l, b, h —thickness, width and the length of the battery. They also observed that with increased discharge rates, the module temperature also increases.

Zhou et al. [162] designed an innovative cooling approach depending on air distribution pipes for the cylindrical li-ion battery. The battery module's 3-D CFD model was created and confirmed the results from the simulations by experimentation. The experimentation is done considering the 18,650-lithium battery of 2 Ah capacity. The rate of heat production is represented by q

$$q = I \left[(V - \text{OCV}) - T \frac{\partial \text{OCV}}{\partial T_a} \right] \quad (47)$$

Here, I is the discharge current, OCV is the open circuit voltage, V is the voltage. $\frac{\partial \text{OCV}}{\partial T_a}$ is the entropy coefficient of the battery, respectively.

The orifices with a diameter of 1 mm, 1.5 mm, and 2 mm are introduced in rows 3, 4, and 5, respectively. Further, they performed the computational analysis considering the frame region to speed up and reduce the time for computation. The coupled flow field and thermal field analysis were performed using finite volume based FLUENT 18.1, and grids

were produced using ICEM 18.1. They used the staggered grid to discretize the governing partial differential equations. SIMPLEC algorithm was used to obtain the pressure terms. Further, they also performed the grid independence test by considering the maximum cell temperature. Furthermore, they marked the battery, namely C1, C2, and C3, to track the variation of battery temperature. The simulation was performed on the Intel i7 CPU with 5 cores considering the boundary conditions with the time step size of 1 s and discharge time of 1200 s. The following boundary conditions were considered.

$$\frac{\partial(\rho_a)}{\partial t} + \nabla \cdot (\rho_a \vec{v}) = 0 \quad (48)$$

$$\frac{\partial(\rho_a \vec{v})}{\partial t} + \nabla \cdot (\rho_a \vec{v} \vec{v}) = -\nabla P \quad (49)$$

$$\frac{\partial(\rho_a C_{Pa} T_a)}{\partial t} + \nabla \cdot (\rho_a C_{Pa} \vec{v} T_a) = \nabla \cdot (k_a \nabla T_a) \quad (50)$$

Here ρ_a —density, C_{Pa} —specific heat, k_a —coefficient of thermal conductivity, T_a —temperature, and P —static pressure of the air. The simulation was executed in 14 h and results were obtained for effect of orifice parameters (diameters and rows), Inlet pressure and discharge on temperature profile of the battery. After examination, they concluded that the proposed air distribution pipe could achieve the required cooling performance at the flow rate of 3 C. Moreover, they emphasize the importance of choosing different inlet pressure for different discharge rates to monitor temperature variation efficiently. Since if the inlet pressure is raised at the discharge of 3 C, a battery module's temperature is shown to drop significantly. Further, they also observed the requirement of higher heat dissipation at higher discharge rates, leading to high power consumption. Ye et al. [79] performed a numerical analysis of the performance of Li-ion battery cells/packs subjected to a HP-TMS during fast charging of the batteries. The simulation was carried out using Ansys CFX 2015, a commercially available CFD code that uses the finite volume approach to describe and evaluate PDE as algebraic equations. Volume integrals in a PDE were modified into surface integrals by the divergence theorem. The discretization of the domain into control volumes was performed by adopting a vertex-centered approach. Different arrangements are used for cooling purposes, such as the use of a vortex generator in the condenser unit, the number of HPs, and fins. The use of fins along with copper spreaders drastically increases the heat transfer capability of HPTMS. It generally consists of an inner wick and vapor core along with condenser and evaporator sections. Three different

designs used for BTM (a) indicate the HPs without fins, (b) indicate HPs with large pitched fins, and (c) indicate the greater number of fins with smaller pitches.

In a similar study made by Wan [152], the temperature distribution ratio in battery systems is reported numerically. The problem is simulated using the commercial Ansys Fluent 17.2 tool. Three factors were used: battery power input, fluid discharge, and its intake temperature. The findings of this investigation demonstrate that battery's temperature distribution can vary both with and without HPs. From the temperature distribution contours, the temperature gradient is observed in only a longitudinal direction in the case of copper rods. While using a HP, more heat is transported from the battery surface since the temperature gradient is evident in both the longitudinal and lateral directions. A numerical simulation of multistage heating of Li-ion batteries was carried out by Sun et al. [163] in cold conditions for efficient working of railway. At different locations, the different heating power is applied while the overall power supply is kept constant. The results obtained demonstrate that the traction battery system can improve battery performance and shorten heating time through multistage heating. The numerical study gives an idea to design a battery pack and matching of heating system. The heating time of model 3 is greater than that of model 2 by 20 s, while the temperature difference between models 1 and 2 is about 0.74 °C. A Li-ion battery characterized by the high discharge rate and cooled by HPs and a thermoelectric cooling device was numerically simulated by Zhang et al. [164]. For the HPs, a material with an enhanced properties is selected to effectively transfer the heat produced by the battery cell's surface. According to the study's findings, using HPs is sufficient to keep the battery system's temperature well within proper range for a medium level of discharge, but using a thermoelectric cooler for a high level of discharge is preferable.

Ye et al. [79] enhanced the existing HP-based TMS using numerical and experimental methods for fast-charging li-ion batteries. The TMS consists of a HP cooling plate (HPCP) to dissipate battery heat produced during the charging and discharging course. The mathematical model was prepared, and the outcomes were validated with test data. The results obtained from the numerical studies illustrate the efficacy of the HP-based TMS or HPTMS. After analyzing the results, they concluded that temperature uniformity is not influenced by altering the number of HPs in HPCP. Moreover, they observed a considerable progress in HPTMS's thermal performance after installing copper heat spreaders and fins due to increased cooling capacity and uniformity in temperature. In Table 5, the scientific studies carried out using heat pipes for efficient BTMS are summarized.

Table 5 Summary of numerical studies using heat pipes for efficient BTMS

Battery geometry	Input Parameters	Analyzed parameter	Coolant used with heat pipe	Remarks	Reference
Prismatic battery cell	Coolant inlet temperature, power input, and coolant flow rate	Peak temperature in the battery cell, External temperature, Temperature difference between the cells	Sintered copper with liquid water	Better control over the Peak battery surface temperature with good temperature uniformity is obtained for the HPs as compared to copper rods	[153]
Prismatic battery cell	Charged capacity, Different design of heat pipe cooling plate, Air cooling, water cooling	Maximum cell temperature, Temperature difference,	Water	The thermal uniformity among the battery cells may not be achieved just by increasing the number of HPs but can be improved by employing a vortex generator at the condenser side. The proposed HPTMS can withstand and work satisfactorily up to a maximum charge rate of 8C. The use of air forced convection system may be effective for each cell but may not be suitable for pack or module	[79]
Prismatic Battery cell	Inlet ambient temperature, flow rate of fluid, charging load	Core temperature of battery pack, surface temperature, Maximum temperature	Water	The battery pack's suggested cooling framework is better suited to regulating the temperature of the battery core within the limit and the cooling modes used in this study are easily adoptable for different ambient temperatures	[157]
Prismatic battery cell	Coolant inlet temperature, power input, and coolant discharge rate	Local Temperature distribution in battery, Peak battery temperature	Sintered copper with water	The battery surface's temperature distribution contours distinctly demonstrate improved homogeneity	[152]
Prismatic battery	Transient condition, State of charge, Current density	Temperature, Volume fraction of liquid in heat pipe, thermal runaway propagation	Water	It is impossible to regulate the thermal runaway in a single battery using an HP cooling system, but the propagation of thermal runaway in an adjacent battery can be easily controlled	[158]
Prismatic battery cell	Transient 1-D, 3-D Numerical simulation, with different discharge current	Maximum surface temperature, Temperature difference	Ammoniac	In comparison to forced convection, a higher amount of HT is made possible by rising the surface area of contact between the HPs and the battery cell	[159]
Prismatic battery cell	Fixed Heat Load, Variable Heat Load without uncertainty, and Variable Heat Load with uncertainty	Battery Temperature, Weight of LHP, Variance of Temperature	Ammonia	With variable heat load and uncertainty, battery performance can be improved drastically, and battery longevity also increases	[82]

Table 5 (continued)

Battery geometry	Input Parameters	Analyzed parameter	Coolant used with heat pipe	Remarks	Reference
Prismatic battery module	Coolant inlet temperature, Coolant flow rate	Battery module temperature, Temperature difference, Li-ion concentration, current and voltage density	Water with sintered copper powder	The battery module temperature reduces, and the local temperature difference increases at the early stage of coolant flow. And as the flow progresses, the temperature difference decreases. The local current density is significantly affected by low coolant temperatures and Li-ion concentration. The available voltage for the battery module declines at low temperature of the coolant, thus decreasing the battery capacity	[154]
Cylindrical battery module	Conduction element height and thickness, battery cell spacing and angle between battery and conduction element, Discharge rate	Maximum battery cell temperature, Temperature difference	Sintered copper water	The obtained results show that the optimal model gives the best temperature distribution contours, out of which the Peak temperature is 27.62 °C, and a temperature variance of 1.08 °C	[156]
Prismatic Battery cell	Heating power, Charge and Discharge rate	Temperature of battery system, temperature difference between the models	Water	A multistage heating system is very useful for high-speed train traction systems to start in low-temperature conditions. The driving range also gets improved	[163]
Prismatic battery cell	Discharge Rate, TEC initial temperature	Battery surface temperature	Water	Use of HP and TEC combined can improve the battery performance and keep the battery surface temperature well below acceptable range. The required discharge rate of BTMS for HP + TEC condition is around 2.5C to 3C	[164]
Prismatic battery cell	Steady and dynamic condition, Discharge rate MHPA and single battery pack cooling	Battery temperature. Temperature gradient	Water	Relying on natural convection for cooling may not be adequate in managing the temperature rise of high energy density batteries when they are subject to a high rate of discharge. MHPA shows excellent performance in controlling the battery temperature within 40 °C	[151]

Experimental and numerical study on HPs

Shah et al. [165] carried out both experimental and numerical investigations of cylindrical Li-ion battery cell generating heat and cooled by heat pipes. A finite element model is constructed with the Ansys CFX tool. An annular air channel along with heat pipes is used for cooling the battery cell. The annular channel was used to study how Li-ion battery cooling works. For experimental purposes, they fabricated the thermal test cells filled with poly-dimethyl siloxane similar in dimensions to 26,650 lithium-ion cells and equivalent thermal properties and performed two sets of experiments. In the first experiment, they passed the coolant air through the annular tube to measure its effectiveness, and in the second set of experiments, they investigated the passive cooling of cells by inserting two copper heat pipes into the metal tubing to acquire the heat from the whole length of the cell. The experiment was performed by suspending the test cell in the wind tunnel such that the condenser end protrudes out of the tunnel and using an air blower for convection of the heat from the protruded tip. Experiments were carried out considering two ambient conditions (Free and Forced convection). The test results for the impact of various internal flow rates on temperature distribution of test cells considering the heating current of 15 A and diameter 2 mm and 6 mm for the inner tubes with a fixed heat generation of 1.62 W. With the use of such a cooling system, a temperature reduction of 18–20 °C is observed in the battery core part. It is noted that battery overheating can be easily avoided with a HP when heat production within the battery increases. The use of HPs and copper rods under forced convection conditions gives good results. The test outcomes show the cell's temperature distribution for the embedded HPs with a heat dissipation rate of 1.62W. The data obtained show a significant reduction (3 °C and 17 °C in peak temperature compared to baseline) in test cell temperature with better results in the forced convection case. Moreover, they also performed finite element simulations using ANSYS CFX to validate the experimental results. The simulation was performed by creating the geometry of the test cell, using the appropriate thermal features, and applying the boundary conditions. After performing the experiments and validating the results with the numerical simulation, they concluded that the experiments carried out by them are promising and could not be accessed through other thermal management systems.

Behi et al. [166] carried out both experimental and computational examination on the TM of Li-ion batteries by making use of both air cooling and HPs. The numerical examination was carried out by using FEM based COMSOL Multiphysics. The variational approach was used for

simulation. Before carrying the simulation, the geometry was divided into elements joined by nodes. An optimum mesh based on the grid independence study was chosen to minimize the computational time and maximize the accuracy. Different optimizing parameters are chosen for the study, such as coolant inlet temperature, cell spacing, air velocity, and use of heat pipes with copper sheet (HPCS). They carried out a number of optimization studies to maintain temperature consistency and enhance the cooling of the lithium battery cells. They initially experimented to determine the battery module's temperature under forced and free convection conditions. They also looked into how battery cooling and temperature variations were affected by cell separation, air temperature, and air velocity. At last, HPS and HPCS were added, and their effect on the temperature uniformity and cooling of the battery module was studied. They observed that the temperature uniformity of the battery module was improved and the peak temperature was reduced using HPCS.

Wei et al. [167] suggested an experimental and numerical method to facilitate the cooling strategy used in the BTMS to get a uniform temperature distribution. A COMSOL Multiphysics and STAR CCM+ CFD software are used to simulate the proposed cooling strategy. The switching time for temperature uniformity in a battery module is studied using a reciprocating cooling strategy rather than a unidirectional flow method. The researchers developed a novel approach to improve the temperature uniformity in battery systems called the “reciprocating cooling strategy”. They achieved this by employing a reversible pump to generate a back-and-forth cooling flow. The TMS for the battery was designed accordingly. The findings of the study suggest that the use of a reciprocating cooling method leads to better temperature control in the battery module. Initially, they carried out a simulation using COMSOL to obtain the thermodynamic parameters of the 60 Ah battery. the results were validated by conducting the real time experiments. The equation of the battery module is given by:

$$\rho_b C_{pb} \frac{\partial T}{\partial \tau} = \frac{\partial}{\partial x} \left(\frac{k_b}{c_{pb}} \frac{\partial T}{\partial x} \right) + \frac{\partial}{\partial y} \left(\frac{k_b}{c_{pb}} \frac{\partial T}{\partial y} \right) + \frac{\partial}{\partial z} \left(\frac{k_b}{c_{pb}} \frac{\partial T}{\partial z} \right) + \dot{Q} \quad (51)$$

where ρ_b , C_{pb} , T and k_b —density, specific heat, temperature, and battery module thermal conductivity respectively. The source term \dot{Q} is represented as:

$$\dot{Q} = \frac{Q_{\text{gen}}}{V_b} \quad (52)$$

The numerical experimentation on the proposed BTMS was also carried out using STAR-CCM+ to study the variations in temperature distribution influenced by the switching time of the battery.

Xu et al. [168] carried out a computational and experimental investigation on rectangular Li-ion battery module subjected to a multistage cooling strategy. The cooling method suggested in this study utilizes flat HPs and a liquid cooling channel. Different parameters are studied, such as charging and discharging rate, battery cell heat production rate, and coolant discharge rate. Initially, they carried out experimentation to determine the necessary parameters required for the computational analysis. The experimentation results show the thermodynamic parameters (initial and termination temperature and heating power) of the 42 Ah battery obtained at different discharge rates. The obtained heat power was also used as the basis of the simulation boundary condition. The computational domain of the physical model, which consists of three modules each containing 12 cells and plates flat HPs, two cooling water channels and several coolers. Once the computational domain is prepared, the inlet, outlet, and some other boundary conditions are applied along with the material properties. The inlet boundary conditions are given by:

$$\psi_1|_{x=L} = 0 \tag{53}$$

$$i_1|_{x=0} = i_1|_{x=L} = -i_{app} \tag{54}$$

$$i_1|_{x=\delta_p} = i_1|_{x=\delta_p+\delta_s} = 0 \tag{55}$$

$$i_2|_{x=0} = i_2|_{x=L} = 0 \tag{56}$$

The i_{app} , i_1 , i_2 and ψ_1 is current density, solid current density vector, electrolyte solution phase density vector and solid phase potential respectively. After performing the simulation, the results were obtained. The temperature variation at different discharge rates (0.5, 1, and 2 C) is obtained at the ambient condition of 20 °C. They observed the maximum temperature at the exit of the model and the minimum at the entry. Moreover, the middle of the model's temperature is high due to the accumulation of heat at the mid portion of the module that cannot be transferred to the cooling water. Further, they also analyzed the thermal efficiency of the model at various discharge rate of 1 C and 2 C. For analysis, four different models namely A (model with no cooler), B (two 15W coolers placed at the highest temperature module), C (two 15 W coolers at each module), and D (two 35 W coolers placed at the exit of the module) were considered. They observed that in model A, the heat is accumulated at the module core with a temperature rise of 7.52 °C and internal temperature difference of 4.48 °C. However, these temperature parameters decreased by 2.7 °C and 1.3 °C in model B compared with model A, and significant temperature decrements are observed in model C. A similar trend of results was observed in the case of a discharge rate of 2 C.

They concluded that the number of coolers and their placement could play a crucial role in the model and increase HT efficiency. The results of this study conclude that using the multistage cooling method, the battery module temperature can be regulated and kept within the acceptable range. It can be clearly observed that with a upsurge in the charge rate and time, both temperature difference and rise in temperature increase.

Yaun et al. [161] performed numerical analysis of a rectangular Li-ion battery cell with a self-designed thermal management module (TMM). The TMM system consists of HPs, heat collecting plates, and conducting fins with forced convection. The discharge capacity impact on the battery cell temperature characteristics were examined. The experimental set up used by them consists of HPs of an outer diameter of 6 mm for the primary source of heat transfer along with heat collecting plates and cooling fins made of aluminum alloy 6063 with an average distance of 2 mm between the fins. They used the lithium iron phosphate battery of 10 Ah capacity as the heat source. The temperature characteristics of the TMM-equipped lithium-ion batteries were investigated using the testing system in an enclosed and adiabatic environment. They attached the five k thermocouples to the battery surface at different locations, namely A, B, C, D, and E. The temperature variation of each site was tracked at 2.5 C discharge rate. The five different used locations are sufficient to track the longitudinal variations. Initially, they discussed the thermal issues and the necessity of BTMS of li-ion batteries by showing the variation of surface temperature with the discharge rate. They observed that the higher discharge rate is associated with a higher rate of reactions leading to unavoidable higher battery temperature. They observed the maximum temperature at point A and the minimum at point E because point A is closest to the electrode tab and E is the farthest. They constructed two prototypes, namely model I (with heat collecting plate) and model II (without heat collecting plate). The temperature transients (Time-dependent temperature characteristics) of models I and II. After analysis of the plot, they observed that the values at the ends of temperature transients of the model I exceed the temperature plot of model II by 6 °C. They concluded that using a heat collector can manage the temperature more efficiently. Moreover, they validated the experimental results using the CFD model in the commercial software Icepack. After considering certain assumptions regarding thermal parameters and material properties, the heat transfer, temperature field, and boundary conditions are given by:

$$\rho C_p \frac{\partial T}{\partial t} = \nabla \cdot (K \nabla T) + q \tag{57}$$

$$\rho C_p \frac{\partial T}{\partial t} = \lambda_x \frac{\partial^2 T}{\partial x^2} + \lambda_y \frac{\partial^2 T}{\partial y^2} + \lambda_z \frac{\partial^2 T}{\partial z^2} + q \quad (58)$$

The initial condition is described by the equation below, where T_0 is the initial value

$$T(x, y, z, 0) = T_0 \quad (59)$$

The other boundary condition in each direction is directed by Newton's law of cooling and can be represented as

$$-\lambda_x \frac{\partial T}{\partial x} = \beta(T - T_\infty), x = 0, l \quad (60)$$

$$-\lambda_y \frac{\partial T}{\partial y} = \beta(T - T_\infty), y = 0, b \quad (61)$$

$$-\lambda_z \frac{\partial T}{\partial z} = \beta(T - T_\infty), z = 0, h \quad (62)$$

The parameter β represents the convective HTC, T_∞ is the ambient temperature and l, b, h is the thickness, width and the length of the battery.

Zhang and Wei [169] suggested a flat plate HP passive cooling method to maintain the surface temperature of the battery pack inside the acceptable range and to increase the battery's life. The numerical model of the battery pack is constructed using Unigraphics NX, and simulation is performed using STAR CCM+ commercial software. Initially, they experimented using the battery test station, data acquisition system, and charge and discharge equipment. The battery pack's temperature (maximum and minimum) was measured using T type thermocouple at the discharge rate of 4 C, 6 C, and 8 C. They observed that the maximum temperature rise of the battery pack occurs in case of insulation without any natural convection means to dissipate the heat generated. To deal with this problem, they incorporated the flat heat pipe in the system and studied the effect on thermal management of the system using numerical method. Further, the comparison of temperature variation under different discharge rate was done considering different thermal management modes (Natural convection, Aluminum Plate and Heat pipe). They observed the significant heat dissipation in case of heat pipe than natural convection and aluminum plate. They observed the decrement of 28.1% and 10.3% in the maximum surface temperature considering the case of heat pipe in comparison to natural convection and aluminum plate respectively. Similar trend of results was observed in case of maximum temperature difference at different discharge rates. After careful analysis of the results, they concluded that the proposed TMS could efficiently regulate the temperature rise at high discharge rates while maintaining compactness and low weight.

Zhou et al. [162] carried out an experimental and numerical investigation on a cylindrical cell battery module subjected to cooling by air. A commercial CFD software based on the FVM was used to solve the governing equations. They prepared a 3D CFD model of the battery module and confirmed the results from the simulations by experimentation. The meshing of the geometry model was carried out by ICEM18.1 commercial mesh software. The thermal behavior of the battery module is observed for various discharge rates, orifice parameters, and inlet air pressure. The experimentation was done considering the 18,650-lithium battery of 2 Ah capacity. The rate of heat generation is represented by q

$$q = I \left[(V - \text{OCV}) - T \frac{\partial \text{OCV}}{\partial T_a} \right] \quad (63)$$

Here, I is the discharge current, OCV is the open circuit voltage, V is the voltage and $\frac{\partial \text{OCV}}{\partial T_a}$ is the entropy coefficient of the battery, respectively.

Further, they marked the battery, namely C1, C2, and C3, to track the temperature variation of the battery. The simulation was performed on the intel i7 CPU with 5 cores considering the boundary conditions with the time step size of 1 s and discharge time of 1200 s. The following boundary conditions were considered

$$\frac{\partial(\rho_a)}{\partial t} + \nabla \cdot (\rho_a \vec{v}) = 0 \quad (64)$$

$$\frac{\partial(\rho_a \vec{v})}{\partial t} + \nabla \cdot (\rho_a \vec{v} \vec{v}) = -\nabla P \quad (65)$$

$$\frac{\partial(\rho_a C_{Pa} T_a)}{\partial t} + \nabla \cdot (\rho_a C_{Pa} \vec{v} T_a) = \nabla \cdot (k_a \nabla T_a) \quad (66)$$

The simulation was executed in 14 h, and results were obtained for the effect of orifice parameters (diameters and rows), Inlet pressure, and discharge rate on the temperature profile of the battery. Further, they marked the top, middle, and bottom surfaces of the battery as P, N, and M to track the variation of temperature at these points. They concluded that the proposed air distribution pipe could achieve the required cooling performance at the discharge rate of 3 C and 4 C. Moreover, they emphasize the importance of choosing different inlet pressure for different discharge rates to monitor temperature variation efficiently. Further, they observed the requirement of higher heat dissipation at higher discharge rates leading to high power consumption.

Sepehr Mousavi [170] proposed a new hybrid cooling system integrating PCM and liquid cooling to attain good performance and safety for a prismatic battery pack. Each module of 4 battery cells is inserted between vertically oriented mini-channel cool plates. They found that at 2 C and

3 C discharge rates, the maximum battery temperatures in the hybrid system with three PCM plates were 5.6 K and 16.2 K lower than those without PCM plates. A two-phase pump-assisted loop heat pipe with two parallel evaporators was constructed by Zhang et al. [171] to improve heat transfer performance and fulfil the necessity for numerous heat sources. Ammonia was used as the working fluid, and a biporous wick constructed of sintered nickel particles was used. They found that, raising the heat load and heat sink temperature decreased the evaporator thermal resistance. Four kinds of porous wicks were produced by Guo et al. [172] and used in Heat Pipe to investigate the impact of particle shape and wettability on the heat transfer performance of Heat Pipe from the standpoint of phase separation. Porous wicks were sintered using spherical and dendritic particle copper powder. The capillary performance of dendritic particle wick was shown to be superior to that of spherical particle wick.

In Table 6, the summary of combined experimental and numerical works using heat pipes for BTMS is presented at a glance.

The prime objective of this review article is to comprehensively address the thermal-related challenges in BTMS, subsequently highlighting the significance of heat pipes and PCM material, which are passive cooling methods. This review article gives an insight into the thermal performance of Li-ion batteries used in electric vehicles, HEV or some other heavy vehicles. One can easily understand the challenges and their solution in the thermal maintenance of EV batteries in the form of a single cell, packed, or modules with different geometrical shapes and sizes. An exhaustive survey reported in this paper comes out with some possible and feasible concluding remarks, which are listed below.

- The experimental studies on heat pipe cooling systems primarily focus on structural design changes in heat pipe geometry or battery modules. Though the common aim of all the experimental work is to bring down the surface temperature of Li-ion batteries to a nominal level at a high discharge rate, their approach to achieving their objective is very different. Most of the experimental work addresses that using heat pipes with suitable working fluid can enhance the heat transfer rate from the battery pack.
- The ultimate goal of this experimental work is to provide an economical, compact, and highly efficient cooling system for batteries.
- The numerical investigations elaborated in this paper focus on the best possible tool for predicting the thermal performance of batteries under various operating conditions. Common software tools for numerical simulation purposes are Ansys Fluent, COMSOL Multiphysics, and Star CCM+.
- The major parameters highlighted in numerical studies are the surface temperature of the battery pack or module, temperature uniformity, temperature difference among the different cells, location of the heat pipe in BTMS, the geometry of the cell, and type of working fluid in heat pipe as well as types of atmospheric condition present.
- Phase change material used in improving the battery thermal performance is highly acceptable but in combination with heat pipes. Compared to heat pipes, the combination of PCM and heat pipe gives more efficient and better results in controlling the battery pack's temperature within the desirable limit, enhancing the heat transfer rate, and improving the life span and running of Li-ion batteries.
- Some commonly used PCM materials are paraffin wax and bees wax due to their economic thermos-physical properties.
- Closed loop oscillating heat pipes (CLOHP) or only oscillating heat pipes (OHP) are also used by many researchers in order to determine their thermal capabilities to control the battery temperature.
- The common working fluids used in OHP are water, ethanol, methanol, and acetone, or a binary mixture (a combination of two different working fluids).
- The major outcomes of these studies related to OHP say that the position of OHP, working fluid in OHP, startup temperature of OHP, filling ratio of working fluid in OHP, length of the adiabatic section in OHP, and finally, the number of turns in OHP tube plays a very crucial role.
- Different structural design parameter of heat pipes and OHP has been suggested by many researchers, such as a cross section of the heat pipe, the internal geometry of the heat pipe, the use of different capillary material within the heat pipe, geometrical shapes of the heat pipe, length of condenser and evaporator section in a heat pipe, and use of PCM material at evaporator and condenser section of the heat pipe. All the above-listed structural parameters have to be considered very meticulously.
- The substantial overheating of lithium-ion batteries at high discharge rates affects the battery's performance and can even lead to an explosion.
- Size optimization is also an important issue when it comes to the practical applications of these batteries.
- The gaining popularity of these batteries in the automobile industries for electric vehicles (EVs) and hybrid electric vehicles (HEVs) accelerated the research activities to obtain better performance and safety.
- The majority of the research is carried out using numerical techniques or combining both experimental and numerical methods. However, few experimental analyses combining heat pipes and PCM have been reported so far.

Table 6 Summary of combined experimental and numerical works using heat pipes for BTMS

Battery geometry	Input Parameters	Analyzed parameter	Coolant used with heat pipe	Remarks	Reference
Cylindrical battery cell	Channel size, Forced and natural convection,	Temperature of battery cell, Temperature reduction, Maximum cell temperature	water	The cooling of battery core is an important aspect of the BTMS even 2% energy density loss can cool the battery very effectively	[165]
Cylindrical cell	Cell Spacing, inlet velocity, air ambient temperature, and discharge rate	Maximum temperature, temperature distribution, Temperature difference	Water	A cell spacing of 2 mm is a better choice among the spacing parameter for controlling the maximum cell temperature and uniformity	[166]
Prismatic battery cell	Charging, discharging rate, charging time	Maximum temperature, minimum temperature, temperature difference, and temperature rise in the battery module	Sintered copper liquid	The switching time for the reciprocating flow strategy affects the temperature rise in the battery module, the shorter the switching time lesser is the temperature rise. Changing the switching time can improve the temperature uniformity in the battery module	[167]
Rectangular battery pack	Charging rate, discharging rate, heat generation, flow rate of liquid coolant	Temperature difference and temperature rise	Water	At a low discharge rate, the temperature rise and temperature difference in a battery pack is kept within 2 °C. But at a high discharge rate, the multistage cooling strategy may have adverse effects,	[168]
Rectangular battery cell	Discharge capacity, Different shapes of heat pipes such as single straight, double straight and U shaped	Temperature, Temperature difference	Water	With the use of heat pipe, heat collecting plate, fins, and forced air convection, it is possible to keep the battery surface temperature within the range of 35.5 °C	[161]
Rectangular battery module	Discharge rate, Current rate, Heat generation rate, Discharge time	Maximum temperature, maximum temperature difference	Water	The use of a heat pipe cooling system adds many advantages to the thermal management system, such as less weight, compactness, and better control of the maximum temperature of the battery module within 40 °C	[169]
Cylindrical cell battery module	Discharge rate, orifice diameter, inlet pressure of air, DOD	Maximum temperature, Temperature difference, Power consumption, Heat removed	Air	The proposed pipe-type air flow cooling system is suitable for battery modules with a discharge rate of 3 C and 4 C, while for 5 C discharge capacity, a very high heat dissipation rate is required	[162]

- The numerical analyses are carried out using computational software like ANSYS FLUENT, COMSOL Multiphysics, MATLAB, ANSYS CFX, and Icepack.
- In general, the trend of determining the thermodynamic parameters using experimental setups was observed as the initial move. Later, the numerical models incorporating the proposed element (heat pipe, air distribution pipe, reversible heat pump) were created, and simulation was performed to monitor the effect of incorporating elements on the thermodynamic parameters.
- Many articles have reported that incorporating heat pipes can efficiently combat the battery's rising surface temperatures at a high discharge rate.
- In some cases, they have coupled heat pipe with a liquid cooling or metal (aluminum) plate and, in others, an annular channel used in the battery's thermal management system.
- However, it is also reported that these cooling systems and heat pipes cannot guarantee to fulfill the automobile industries' demands at high discharge rates.
- Considerable research still needs to improve the battery's performance to use it to its full potential. We believe this comprehensive review will undoubtedly benefit the current researchers and designers from various organizations and industries.
- Developing heat pipes for high-temperature applications: many batteries generate high temperatures during operation. Developing heat pipes that can effectively remove heat at these high temperatures is an ongoing challenge.
- Optimizing the geometry of heat pipes: The geometry of heat pipes can affect their performance. So many researchers are working to optimize the geometry of heat pipes to improve their thermal management capabilities.
- Integration of heat pipes into battery packs: The integration of heat pipes into battery packs is still a challenge. Researchers are working on making the heat pipes more compact and lightweight for better integration into battery packs.
- Increasing the area of heat transfer between the heat source, the heat pipe, and the heat sink while also enhancing the efficiency using various techniques like incorporating PCM, nanofluids in HP integrated BTMS.
- Examining how heat pipes work and how limited they are when subjected to extremely quick charging, changing heat loads, and multiple heat loads.
- Another potential research gap in BTMS using heat pipes is the integration of machine learning (ML) techniques to optimize the performance of the thermal management system. While some research has been done on using ML algorithms to predict and control battery temperature, there is a lack of studies on the application of these techniques to heat pipe systems specifically.
- Machine learning could be used to optimize the operation of heat pipes by predicting and controlling the flow of heat, improving the efficiency and effectiveness of the thermal management system.
- Additionally, machine learning could be used to monitor the performance of the heat pipe system over time and adjust the system to adapt to changes in battery temperature and usage patterns. Further research in this area could lead to more intelligent and adaptable thermal management systems for batteries.
- Soft computing techniques are becoming important because of their low processing cost and ability to examine a wide variety of factors to identify the best solutions. These techniques are ideal for determining the optimal configuration of design parameters and operational settings to maximize BTMS performance.

Future scope

Although there have been decades of study in this area, heat pipe-based BTMS have not yet reached the commercialization stage. The following areas need further investigation in order to determine if heat pipes may be used in thermal management batteries.

- The lack of studies on the long-term performance and durability of heat pipe systems in high-temperature and high-power battery applications. Many studies have focused on the initial performance of heat pipe systems in laboratory settings, but there is a need for more research on the long-term reliability and effectiveness of these systems in real-world applications.
- Additionally, there is a lack of research on the optimization of heat pipe design and materials for specific battery chemistries and thermal management requirements. Further research in these areas could lead to more efficient and durable heat pipe systems for battery thermal management.
- Improving the thermal conductivity and heat transfer coefficient of heat pipes: Current heat pipe designs have relatively low thermal conductivity and heat transfer coefficient, which can limit their effectiveness in removing heat from batteries.

Acknowledgements This study was financially supported by Seoul National University of Science and Technology.

Authors Contribution AA performed Writing original draft, conceptualization, and methodology. MSAD done Writing original draft, Software, and Editing the Manuscript. KAR did Writing original draft, conceptualization, and methodology. RK performed Writing original draft, conceptualization, and methodology. ÜA did Reviewing, Resources & Supervision. SGP done Resources & Supervision, Drafting

Declarations

Conflict of interest None.

References

- Said Z, Sharma P, Elavarasan RM, Tiwari AK, Rathod MK. Exploring the specific heat capacity of water-based hybrid nano-fluids for solar energy applications: A comparative evaluation of modern ensemble machine learning techniques. *J Energy Storage*. 2022;54:105230.
- Afzal A, Samee ADM, Razak RKA, Ramis MK. Effect of spacing on thermal performance characteristics of Li-ion battery cells. *J Therm Anal Calorim*. 2019;135:1797–811.
- Mokashi I, Khan SA, Abdullah NA, Bin Azami MH, Afzal A. Maximum temperature analysis in a Li-ion battery pack cooled by different fluids. *J Therm Anal Calorimetry*. 2020;141:2555–71.
- Petroleum B. Statistical review of world energy 2009. London: BP; 2009.
- Andersen PH, Mathews JA, Rask M. Integrating private transport into renewable energy policy: the strategy of creating intelligent recharging grids for electric vehicles. *Energy Policy*. 2009;37:2481–6.
- Birol F. World energy outlook. Paris Int Energy Agency. 2008;23:329.
- Han L, Zhou W, Li W, Meshesha DT, Li L, Zheng M. Meteorological and urban landscape factors on severe air pollution in Beijing. *J Air Waste Manage Assoc*. 2015;65:782–7.
- Afzal A, Ramis MK. Multi-objective optimization of thermal performance in battery system using genetic and particle swarm algorithm combined with fuzzy logics. *J Energy Storage*. 2020;32:101815.
- Afzal A, Mohammed Samee AD, Abdul Razak RK, Ramis MK. Thermal management of modern electric vehicle battery systems (MEVBS). *J Therm Anal Calorim*. 2020. <https://doi.org/10.1007/s10973-020-09606-x>.
- Pesaran AA. Battery thermal management in EV and HEVs: issues and solutions. *Battery Man*. 2001;43(5):34–49.
- Rao Z, Wang S. A review of power battery thermal energy management. *Renew Sustain Energy Rev*. 2011;15:4554–71.
- Ritchie A, Howard W. Recent developments and likely advances in lithium-ion batteries. *J Power Sources*. 2006;162:809–12.
- Etacheri V, Marom R, Elazari R, Salitra G, Aurbach D. Challenges in the development of advanced Li-ion batteries: a review. *Energy Environ Sci*. 2011;4:3243–62.
- Doughty DH, Roth EP. A general discussion of Li ion battery safety. *Electrochem Soc Interface*. 2012;21:37.
- Waldmann T, Wilka M, Kasper M, Fleischhammer M, Wohlfahrt-Mehrens M. Temperature dependent ageing mechanisms in Lithium-ion batteries—a post-mortem study. *J Power Sources*. 2014;262:129–35.
- Motloch CG, Belt JR, Christophersen JP, Wright R Ben, Hunt GL, Haskind HJ, et al. PNGV Battery Testing Procedures and Analytical Methodologies for Hybrid Electric Vehicles. Idaho National Laboratory (INL); 2002.
- Huo Y, Rao Z. Investigation of phase change material based battery thermal management at cold temperature using lattice Boltzmann method. *Energy Convers Manag*. 2017;133:204–15.
- Afzal A, Samee ADM, Jilte RD, Islam MT, Manokar AM, Razak KA. Battery thermal management: an optimization study of parallelized conjugate numerical analysis using Cuckoo search and Artificial bee colony algorithm. *Int J Heat Mass Transf*. 2021;166:120798.
- Jilte R, Afzal A, Panchal S. A novel battery thermal management system using nano-enhanced phase change materials. *Energy*. 2021;219:119564. <https://doi.org/10.1016/j.energy.2020.119564>.
- Kizilel R, Sabbah R, Selman JR, Al-Hallaj S. An alternative cooling system to enhance the safety of Li-ion battery packs. *J Power Sources*. 2009;194:1105–12.
- Waag W, Käbitz S, Sauer DU. Experimental investigation of the lithium-ion battery impedance characteristic at various conditions and aging states and its influence on the application. *Appl Energy*. 2013;102:885–97.
- Ramadass P, Haran B, White R, Popov BN. Capacity fade of Sony 18650 cells cycled at elevated temperatures: part II. Capacity fade analysis. *J Power Sources*. 2002;112:614–20.
- Jhu C-Y, Wang Y-W, Wen C-Y, Shu C-M. Thermal runaway potential of LiCoO₂ and Li(Ni_{1/3}Co_{1/3}Mn_{1/3})O₂ batteries determined with adiabatic calorimetry methodology. *Appl Energy*. 2012;100:127–31.
- Catherino HA. Complexity in battery systems: thermal runaway in VRLA batteries. *J Power Sources*. 2006;158:977–86.
- Lin H-P, Chua D, Salomon M, Shiao HC, Hendrickson M, Plichta E, et al. Low-temperature behavior of Li-ion cells. *Electrochem Solid State Lett*. 2001;4:A71.
- Khateeb SA, Amiruddin S, Farid M, Selman JR, Al-Hallaj S. Thermal management of Li-ion battery with phase change material for electric scooters: experimental validation. *J Power Sources*. 2005;142:345–53.
- Pesaran AA, Vlahinos A, Burch SD. Thermal performance of EV and HEV battery modules and packs. National Renewable Energy Laboratory; 1997.
- Soudagar MEM, Kalam MA, Sajid MU, Afzal A, Banapurmath NR, Akram N, et al. Thermal analyses of minichannels and use of mathematical and numerical models. *Numer Heat Transf Part A Appl*. 2020;77:497–537. <https://doi.org/10.1080/10407782.2019.1701883>.
- Afzal A, Samee ADM, Razak RKA, Ramis MK. Steady and transient state analyses on conjugate laminar forced convection heat transfer. *Arch Comput Methods Eng*. 2020;27:135–70. <https://doi.org/10.1007/s11831-018-09303-x>.
- Afzal A, Mohammed Samee AD, Abdul Razak RK, Ramis MK. Effect of spacing on thermal performance characteristics of Li-ion battery cells. *J Therm Anal Calorimetry*. 2019;135(3):1797–811. <https://doi.org/10.1007/s10973-018-7664-2>.
- Samee AM, Afzal A, Ramis MK, Razak RA. Optimal spacing in heat generating parallel plate channel: a conjugate approach. *Int J Therm Sci*. 2019;136:267–77. <https://doi.org/10.1016/j.jithe rmalsci.2018.10.025>.
- Zhao C, Sousa ACM, Jiang F. Minimization of thermal non-uniformity in lithium-ion battery pack cooled by channeled liquid flow. *Int J Heat Mass Transf*. 2019;129:660–70. <https://doi.org/10.1016/j.jheatmasstransfer.2018.10.017>.
- Al-Zareer M, Dincer I, Rosen MA. A review of novel thermal management systems for batteries. *Int J Energy Res*. 2018;42:3182–205. <https://doi.org/10.1002/er.4095>.
- Kim J, Oh J, Lee H. Review on battery thermal management system for electric vehicles. *Appl Therm Eng*. 2019;149:192–212. <https://doi.org/10.1016/j.applthermaleng.2018.12.020>.
- Selimefendigil F, Öztop HF, Abu-Hamdeh N. Optimization of phase change process in a sinusoidal-wavy conductive walled cylinder with encapsulated-phase change material during magnetohydrodynamic nanofluid convection. *J Energy Storage*. 2022;55:105512.
- Aich W, Selimefendigil F, Alqahtani T, Algarni S, Alshehry S, Kolsi L. Thermal and phase change process in a locally curved open channel equipped with PCM-PB and heater during nanofluid convection under magnetic field. *Mathematics*. 2022;10:4070.

37. Omri M, Selimefendigil F, Smaoui HT, Kolsi L. Cooling system design for photovoltaic thermal management by using multiple porous deflectors and nanofluid. *Case Stud Therm Eng.* 2022;39:102405.
38. Selimefendigil F, Öztıp HF. Performance assessment of a thermoelectric module by using rotating circular cylinders and nanofluids in the channel flow for renewable energy applications. *J Clean Prod.* 2021;279:123426.
39. Okulu D, Selimefendigil F, Öztıp HF. Review on nanofluids and machine learning applications for thermoelectric energy conversion in renewable energy systems. *Eng Anal Bound Elem.* 2022;144:221–61.
40. Selimefendigil F, Öztıp HF. Identification of pulsating flow effects with CNT nanoparticles on the performance enhancements of thermoelectric generator (TEG) module in renewable energy applications. *Renew Energy.* 2020;162:1076–86.
41. Selimefendigil F, Öztıp HF. Thermoelectric generation from vented cavities with a rotating conic object and highly conductive CNT nanofluids for renewable energy systems. *Int Commun Heat Mass Transf.* 2021;122:105139.
42. Selimefendigil F, Öztıp HF, Afrand M. Shape effects of TEG mounted ventilated cavities with alumina-water nanofluids on the performance features by using artificial neural networks. *Eng Anal Bound Elem.* 2022;140:79–97.
43. Arora S. Selection of thermal management system for modular battery packs of electric vehicles: a review of existing and emerging technologies. *J Power Sources.* 2018;400:621–40.
44. Yang X, Yan YY, Mullen D. Recent developments of lightweight, high performance heat pipes. *Appl Therm Eng.* 2012;33:1–14.
45. Ting CC, Chen CC. Analyzing the heat transfer property of heat pipe influenced by integrated cooling apparatus. *Life.* 2014;20000(30000):40000.
46. Haro S, Ramírez C, Mendoza E, Rodríguez J, Colás R. Microstructural analysis of heat-resistant welded pipes. *Mater Charact.* 2003;51:21–7. <https://doi.org/10.1016/j.matchar.2003.09.005>.
47. Lu W, Zhao CY, Tassou SA. Thermal analysis on metal-foam filled heat exchangers. Part I: metal-foam filled pipes. *Int J Heat Mass Transf.* 2006;49:2751–61.
48. Xiao B, Faghri A. A three-dimensional thermal-fluid analysis of flat heat pipes. *Int J Heat Mass Transf.* 2008;51:3113–26. <https://doi.org/10.1016/j.ijheatmasstransfer.2007.08.023>.
49. Tardy F, Sami SM. Thermal analysis of heat pipes during thermal storage. *Appl Therm Eng.* 2009;29:329–33. <https://doi.org/10.1016/j.applthermaleng.2008.02.037>.
50. Nithyanandam K, Pitchumani R. Analysis and optimization of a latent thermal energy storage system with embedded heat pipes. *Int J Heat Mass Transf.* 2011;54:4596–610. <https://doi.org/10.1016/j.ijheatmasstransfer.2011.06.018>.
51. Lips S, Lefèvre F, Bonjour J. Physical mechanisms involved in grooved flat heat pipes: experimental and numerical analyses. *Int J Therm Sci.* 2011;50:1243–52. <https://doi.org/10.1016/j.ijthermalsci.2011.02.008>.
52. Chi SW. Heat pipe theory and practice. Hemi. 1976.
53. Shukla KN. Heat pipe for aerospace applications—An overview 2015. *J Electron Cool Therm Cont.* 2015;5:1–14. <https://doi.org/10.4236/jectc.2015.51001>
54. Shabgard H, Robak CW, Bergman TL, Faghri A. Heat transfer and exergy analysis of cascaded latent heat storage with gravity-assisted heat pipes for concentrating solar power applications. *Sol Energy.* 2012;86:816–30. <https://doi.org/10.1016/j.solener.2011.12.008>.
55. Liu X, Chen Y. Transient thermal performance analysis of micro heat pipes. *Appl Therm Eng.* 2013;58:585–93. <https://doi.org/10.1016/j.applthermaleng.2013.04.025>.
56. Anderson WG, Hartenstine J, Ellis M, Montgomery J, Peters C. Electronics cooling using high temperature loop heat pipes with multiple condensers. Fort Worth, TX: Power System Conference; 2010. p. 2–4.
57. Zemlianyov P, Combes C. Thermal control of space electronics. *Electron Cool.* 1996;2:24–9.
58. Priester DE. Transient response of a cryogenic heat pipe 1976.
59. RANKIN J. Integration and flight demonstration of a high-capacity monogroove heat-pipe radiator. 19th Thermophysics Conference 1984. p. 1716.
60. BRENNAN P, Thienel LEE, Swanson TED, Morgan M. Flight data for the cryogenic heat pipe (CRYOHP) experiment. 28th Thermophysics Conference 1993. p. 2735.
61. Garner SD. Heat pipes for electronics cooling applications. *Electron Cool.* 1996;2:18–23.
62. Sajjad U, Hamid K, Sultan M, Abbas N, Ali HM, Imran M, et al. Personal thermal management-A review on strategies, progress, and prospects. *Int Commun Heat Mass Transf.* 2022;130:105739.
63. Barrak A. Heat pipes heat exchanger for HVAC applications. In *Heat transfer-design, experimentation and applications 2021*. IntechOpen.
64. Peng H, Pai PF, Ma H. Nonlinear thermomechanical finite-element modeling, analysis and characterization of multi-turn oscillating heat pipes. *Int J Heat Mass Transf.* 2014;69:424–37. <https://doi.org/10.1016/j.ijheatmasstransfer.2013.10.041>.
65. Fang T, Ming T, Tso CP, Huang X, Liu W. Analysis of non-uniform heat loads on evaporators with loop heat pipes. *Int J Heat Mass Transf.* 2014;75:313–26. <https://doi.org/10.1016/j.ijheatmasstransfer.2014.03.061>.
66. Bai L, Zhang L, Lin G, He J, Wen D. Development of cryogenic loop heat pipes: a review and comparative analysis. *Appl Therm Eng.* 2015;89:180–91. <https://doi.org/10.1016/j.applthermaleng.2015.06.010>.
67. Fairley JD, Thompson SM, Anderson D. Time–frequency analysis of flat-plate oscillating heat pipes. *Int J Therm Sci.* 2015;91:113–24. <https://doi.org/10.1016/j.ijthermalsci.2015.01.001>.
68. Li J, Zhu Z, Zhu Z. Battery thermal management systems of electric vehicles 2014:79.
69. Liu Y, Yang S, Guo B, Deng C. Numerical analysis and design of thermal management system for lithium ion battery pack using thermoelectric coolers. *Adv Mech Eng.* 2014;6:852712.
70. Saw LH, Somasundaram K, Ye Y, Tay AAO. Electro-thermal analysis of lithium iron phosphate battery for electric vehicles. *J Power Sources.* 2014;249:231–8.
71. Gan Y, He L, Liang J, Tan M, Xiong T, Li Y. A numerical study on the performance of a thermal management system for a battery pack with cylindrical cells based on heat pipes. *Appl Therm Eng.* 2020;179:115740. <https://doi.org/10.1016/j.applthermaleng.2020.115740>.
72. Jiite RD, Kumar R. Numerical investigation on cooling performance of Li-ion battery thermal management system at high galvanostatic discharge. *Eng Sci Technol an Int J.* 2018;21:957–69. <https://doi.org/10.1016/j.jestch.2018.07.015>.
73. Selimefendigil F, Öztıp HF. Optimization assisted CFD for using double porous cylinders on the performance improvement of TEG mounted 3D channels. *Sustain Energy Technol Assessments.* 2022;52:102303.
74. Selimefendigil F, Öztıp HF. Thermoelectric generation in bifurcating channels and efficient modeling by using hybrid CFD and artificial neural networks. *Renew Energy.* 2021;172:582–98.
75. Aich W, Selimefendigil F, Ayadi B, Ben Said L, Alshammari BM, Kolsi L, et al. Application and CFD-based optimization of a novel porous object for confined slot jet impingement cooling systems under a magnetic field. *Mathematics.* 2022;10:2578.
76. Saw LH, Ye Y, Tay AAO, Chong WT, Kuan SH, Yew MC. Computational fluid dynamic and thermal analysis of Lithium-ion

- battery pack with air cooling. *Appl Energy*. 2016;177:783–92. <https://doi.org/10.1016/j.apenergy.2016.05.122>.
77. Huang G, Liu W, Luo Y, Li Y. A novel ultra-thin vapor chamber for heat dissipation in ultra-thin portable electronic devices. *Appl Therm Eng*. 2020;167:114726.
 78. Weibel JA, Garimella SV, North MT. Characterization of evaporation and boiling from sintered powder wicks fed by capillary action. *Int J Heat Mass Transf*. 2010;53:4204–15.
 79. Ye Y, Saw LH, Shi Y, Tay AAO. Numerical analyses on optimizing a heat pipe thermal management system for lithium-ion batteries during fast charging. *Appl Therm Eng*. 2015;86:281–91.
 80. Poplaski LM, Faghri A, Bergman TL. Analysis of internal and external thermal resistances of heat pipes including fins using a three-dimensional numerical simulation. *Int J Heat Mass Transf*. 2016;102:455–69. <https://doi.org/10.1016/j.ijheatmasstransfer.2016.05.116>.
 81. Ersöz MA, Yildiz A. Thermoeconomic analysis of thermosiphon heat pipes. *Renew Sustain Energy Rev*. 2016;58:666–73. <https://doi.org/10.1016/j.rser.2015.12.250>.
 82. Park YJ, Jun S, Kim S, Lee DH. Design optimization of a loop heat pipe to cool a lithium ion battery onboard a military aircraft. *J Mech Sci Technol*. 2010;24:609–18. <https://doi.org/10.1007/s12206-009-1214-6>.
 83. Wang X, Zhu Y, Zhu M, Zhu Y, Fan H, Wang Y. Thermal analysis and optimization of an ice and snow melting system using geothermy by super-long flexible heat pipes. *Appl Therm Eng*. 2017;112:1353–63. <https://doi.org/10.1016/j.applthermaleng.2016.11.007>.
 84. Daimaru T, Yoshida S, Nagai H. Study on thermal cycle in oscillating heat pipes by numerical analysis. *Appl Therm Eng*. 2017;113:1219–27. <https://doi.org/10.1016/j.applthermaleng.2016.11.114>.
 85. Chi RG, Chung WS, Rhi SH. Thermal characteristics of an oscillating heat pipe cooling system for electric vehicle li-ion batteries. *Energies*. 2018;11(3):655.
 86. Fasula C. Oscillating heat pipes (OHP). Master of Science in Mechanical Engineering and Applied Mechanics, University of Rhode Island 2009.
 87. Qu J, Ke Z, Zuo A, Rao Z. Experimental investigation on thermal performance of phase change material coupled with three-dimensional oscillating heat pipe (PCM/3D-OHP) for thermal management application. *Int J Heat Mass Transf*. 2019;129:773–82. <https://doi.org/10.1016/j.ijheatmasstransfer.2018.10.019>.
 88. Wang X, Wang Y, Wang Z, Liu Y, Zhu Y, Chen H. Simulation-based analysis of a ground source heat pump system using super-long flexible heat pipes coupled borehole heat exchanger during heating season. *Energy Convers Manag*. 2018;164:132–43. <https://doi.org/10.1016/j.enconman.2018.03.001>.
 89. Azad E. Experimental analysis of thermal performance of solar collectors with different numbers of heat pipes versus a flow-through solar collector. *Renew Sustain Energy Rev*. 2018;82:4320–5. <https://doi.org/10.1016/j.rser.2017.10.015>.
 90. Al-Obaidi AR. Investigation of fluid field analysis, characteristics of pressure drop and improvement of heat transfer in three-dimensional circular corrugated pipes. *J Energy Storage*. 2019;26:101012. <https://doi.org/10.1016/j.est.2019.101012>.
 91. Liu C, Zhang Z. Thermal response of wall implanted with heat pipes: experimental analysis. *Renew Energy*. 2019;143:1687–97. <https://doi.org/10.1016/j.renene.2019.05.123>.
 92. Koito Y. Numerical analyses on heat transfer characteristics of ultra-thin heat pipes: fundamental studies with a three-dimensional thermal-fluid model. *Appl Therm Eng*. 2019;148:430–7. <https://doi.org/10.1016/j.applthermaleng.2018.10.119>.
 93. Allouhi A, Benzakour AM. Effect analysis on energetic, exergetic and financial performance of a flat plate collector with heat pipes. *Energy Convers Manag*. 2019;195:274–89. <https://doi.org/10.1016/j.enconman.2019.04.081>.
 94. Felczak M, de Mey G, Więcek B, Chatzipanagiotou P, Chatziathanasiou V. Dynamic thermal heat pipes analysis: Thermal impedance in start-up condition. *Microelectron J*. 2019;93:104639. <https://doi.org/10.1016/j.mejo.2019.104639>.
 95. Liu FF, Lan FC, Chen JQ, Li YG. Experimental investigation on cooling/heating characteristics of ultra-thin micro heat pipe for electric vehicle battery thermal management. *Chin J Mech Eng*. 2018;31:1–10. <https://doi.org/10.1186/s10033-018-0255-0>.
 96. Reay DA. Thermal energy storage: the role of the heat pipe in performance enhancement. *Int J Low-Carbon Technol*. 2015;10:99–109.
 97. Wu W, Yang X, Zhang G, Chen K, Wang S. Experimental investigation on the thermal performance of heat pipe-assisted phase change material based battery thermal management system. *Energy Convers Manag*. 2017;138:486–92. <https://doi.org/10.1016/j.enconman.2017.02.022>.
 98. Xiaohong G, Xiange S, Miao Z, Dawei T. Influence of void ratio on thermal stress of PCM canister for heat pipe receiver. *Appl Therm Eng*. 2016;94:615–21.
 99. Essa MA, Rofaiei IY, Ahmed MA. Experimental and theoretical analysis for the performance of evacuated tube collector integrated with helical finned heat pipes using PCM energy storage. *Energy*. 2020;206:118166. <https://doi.org/10.1016/j.energy.2020.118166>.
 100. Qu J, Zuo A, Liu F, Rao Z. Quantitative analysis of thermal performance and flow characteristics of oscillating heat pipes with different initial pressure. *Appl Therm Eng*. 2020;181:115962. <https://doi.org/10.1016/j.applthermaleng.2020.115962>.
 101. Markal B, Varol R. Experimental investigation and force analysis of flat-plate type pulsating heat pipes having ternary mixtures. *Int Commun Heat Mass Transf*. 2021;121:105084. <https://doi.org/10.1016/j.icheatmasstransfer.2020.105084>.
 102. Zhao J, Qu J, Rao Z. Thermal characteristic and analysis of closed loop oscillation heat pipe/phase change material (CLOHP/PCM) coupling module with different working media. *Int J Heat Mass Transf*. 2018;126:257–66.
 103. Zhao J, Lv P, Rao Z. Experimental study on the thermal management performance of phase change material coupled with heat pipe for cylindrical power battery pack. *Exp Therm Fluid Sci*. 2017;82:182–8. <https://doi.org/10.1016/j.expthermflusci.2016.11.017>.
 104. Zhao J, Rao Z, Liu C, Li Y. Experiment study of oscillating heat pipe and phase change materials coupled for thermal energy storage and thermal management. *Int J Heat Mass Transf*. 2016;99:252–60.
 105. Yang X-H, Tan S-C, He Z-Z, Liu J. Finned heat pipe assisted low melting point metal PCM heat sink against extremely high power thermal shock. *Energy Convers Manag*. 2018;160:467–76.
 106. Ye Y, Shi Y, Huat L, Tay AAO. Performance assessment and optimization of a heat pipe thermal management system for fast charging lithium ion battery packs. *Int J Heat Mass Transf*. 2016;92:893–903. <https://doi.org/10.1016/j.ijheatmasstransfer.2015.09.052>.
 107. Agyenim F, Hewitt N, Eames P, Smyth M. A review of materials, heat transfer and phase change problem formulation for latent heat thermal energy storage systems (LHTESS). *Renew Sustain Energy Rev*. 2010;14:615–28.
 108. Said Z, Sharma P, Sundar LS, Tran VD. Using Bayesian optimization and ensemble boosted regression trees for optimizing thermal performance of solar flat plate collector under thermosiphon condition employing MWCNT-Fe₃O₄/water hybrid nanofluids. *Sustain Energy Technol Assessments*. 2022;53:102708.
 109. Said Z, Rahman S, Sharma P, Hachicha AA, Issa S. Performance characterization of a solar-powered shell and tube heat exchanger

- utilizing MWCNTs/Water-based nanofluids: an experimental, numerical, and artificial intelligence approach. *Appl Therm Eng* 2022;118633.
110. Said Z, Sharma P, Sundar LS, Afzal A, Li C. Synthesis, stability, thermophysical properties and AI approach for predictive modelling of Fe₃O₄ coated MWCNT hybrid nanofluids. *J Mol Liq*. 2021;340:117291.
 111. Said Z, Sundar LS, Tiwari AK, Ali HM, Sheikholeslami M, Bellos E, et al. Recent advances on the fundamental physical phenomena behind stability, dynamic motion, thermophysical properties, heat transport, applications, and challenges of nanofluids. *Phys Rep*. 2022;946:1–94.
 112. Wang Y, Al-Saaidi HAI, Kong M, Alvarado JL. Thermophysical performance of graphene based aqueous nanofluids. *Int J Heat Mass Transf*. 2018;119:408–17.
 113. Huq T, Ong HC, Chew BT, Leong KY, Newaz KS. Review on aqueous graphene nanoplatelet nanofluids: preparation, Stability, thermophysical properties, and applications in heat exchangers and solar thermal collectors. *Appl Therm Eng* 2022;118342.
 114. Sarafraz MM, Yang B, Pourmehran O, Arjomandi M, Ghomashchi R. Fluid and heat transfer characteristics of aqueous graphene nanoplatelet (GNP) nanofluid in a microchannel. *Int Commun Heat Mass Transf*. 2019;107:24–33.
 115. Sharma P, Said Z, Kumar A, Nizetic S, Pandey A, Hoang AT, et al. Recent advances in machine learning research for nanofluid-based heat transfer in renewable energy system. *Energy Fuels*. 2022;36:6626–58.
 116. Wu M, Liu K, Wang Y, Wan CC. Heat dissipation design for lithium-ion batteries. *J Power Sources*. 2002;109:160–6.
 117. Rao Z, Wang S, Wu M, Lin Z, Li F. Experimental investigation on thermal management of electric vehicle battery with heat pipe. *Energy Convers Manag*. 2013;65:92–7. <https://doi.org/10.1016/j.enconman.2012.08.014>.
 118. Wang H, Wang Y, Hu F, Shi W, Hu X, Li H, et al. Heat generation measurement and thermal management with phase change material based on heat flux for high specific energy power battery. *Appl Therm Eng*. 2021;194:117053.
 119. Tran TH, Harmand S, Desmet B, Filangi S. Experimental investigation on the feasibility of heat pipe cooling for HEV/EV lithium-ion battery. *Appl Therm Eng*. 2014;63:551–8. <https://doi.org/10.1016/j.applthermaleng.2013.11.048>.
 120. Wang Q, Jiang B, Xue QF, Sun HL, Li B, Zou HM, et al. Experimental investigation on EV battery cooling and heating by heat pipes. *Appl Therm Eng*. 2014;88:54–60. <https://doi.org/10.1016/j.applthermaleng.2014.09.083>.
 121. Belyaev A. Investigation of heat pipe cooling of LI- ion batteries. American Society of Thermal and Fluids Engineers (ASTFE) Conference, New York City: 2015.
 122. Liang J, Gan Y, Li Y. Investigation on the thermal performance of a battery thermal management system using heat pipe under different ambient temperatures. *Energy Convers Manag*. 2018;155:1–9.
 123. Maghrabie HM, Olabi AG, Alami AH, Al Radi M, Zwayyed F, Wilberforce T, et al. Numerical simulation of heat pipes in different applications. *Int J Thermofluids*. 2022;16:100199.
 124. Hong S, Zhang X, Wang S, Zhang Z. Experiment study on heat transfer capability of an innovative gravity assisted ultra-thin looped heat pipe. *Int J Therm Sci*. 2015;95:106–14. <https://doi.org/10.1016/j.ijthermalsci.2015.04.003>.
 125. Zhang J, Huang J, Li Z, Wu B, Nie Z, Sun Y, et al. Comparison and validation of methods for estimating heat generation rate of large-format lithium-ion batteries. *J Therm Anal Calorim*. 2014;117:447–61.
 126. Zhao R, Gu J, Liu J. An experimental study of heat pipe thermal management system with wet cooling method for lithium ion batteries. *J Power Sources*. 2015;273:1089–97. <https://doi.org/10.1016/j.jpowsour.2014.10.007>.
 127. Liu F, Lan F, Chen J. Dynamic thermal characteristics of heat pipe via segmented thermal resistance model for electric vehicle battery cooling. *J Power Sources*. 2016;321:57–70. <https://doi.org/10.1016/j.jpowsour.2016.04.108>.
 128. Deng S, Li K, Xie Y, Wu C, Wang P, Yu M, et al. Heat pipe thermal management based on high-rate discharge and pulse cycle tests for lithium-ion batteries. *Energies*. 2019;12:3143. <https://doi.org/10.3390/en12163143>.
 129. Jouhara H, Serey N, Khordehghah N, Bennett R, Almahmoud S, Lester SP. Investigation, development and experimental analyses of a heat pipe based battery thermal management system. *Int J Thermofluids*. 2020;1:100004. <https://doi.org/10.1016/j.ijft.2019.100004>.
 130. Feng L, Zhou S, Li Y, Wang Y, Zhao Q, Luo C, et al. Experimental investigation of thermal and strain management for lithium-ion battery pack in heat pipe cooling. *J Energy Storage*. 2018;16:84–92. <https://doi.org/10.1016/j.est.2018.01.001>.
 131. Smith J, Singh R, Hinterberger M, Mochizuki M. Battery thermal management system for electric vehicle using heat pipes. *Int J Therm Sci*. 2018;134:517–29. <https://doi.org/10.1016/j.ijthermalsci.2018.08.022>.
 132. Ye X, Zhao Y, Quan Z. Experimental study on heat dissipation for lithium-ion battery based on micro heat pipe array (MHPA). *Appl Therm Eng*. 2018;130:74–82. <https://doi.org/10.1016/j.applthermaleng.2017.10.141>.
 133. Ariantara B, Putra N, Supriadi S. Battery thermal management system using loop heat pipe with LTP copper capillary wick. *IOP Conf Ser Earth Environ Sci*. 2018;105:1–6. <https://doi.org/10.1088/1755-1315/105/1/012045>.
 134. Worwood D, Kellner Q, Wojtala M, Widanage WD, McGlen R, Greenwood D, et al. A new approach to the internal thermal management of cylindrical battery cells for automotive applications. *J Power Sources*. 2017;346:151–66. <https://doi.org/10.1016/j.jpowsour.2017.02.023>.
 135. Nemeč P, Čaja A, Malcho M. Mathematical model for heat transfer limitations of heat pipe. *Math Comput Model*. 2013;57:126–36.
 136. Gan Y, Wang J, Liang J, Huang Z, Hu M. Development of thermal equivalent circuit model of heat pipe-based thermal management system for a battery module with cylindrical cells. *Appl Therm Eng*. 2020;164:114523. <https://doi.org/10.1016/j.applthermaleng.2019.114523>.
 137. Zou H, Wang W, Zhang G, Qin F, Tian C, Yan Y. Experimental investigation on an integrated thermal management system with heat pipe heat exchanger for electric vehicle. *Energy Convers Manag*. 2016;118:88–95. <https://doi.org/10.1016/j.enconman.2016.03.066>.
 138. Ye X, Zhao Y, Quan Z. Thermal management system of lithium-ion battery module based on micro heat pipe array. *Int J Energy Res*. 2018;42:648–55. <https://doi.org/10.1002/er.3847>.
 139. Putra N, Ariantara B, Pamungkas RA. Experimental investigation on performance of lithium-ion battery thermal management system using flat plate loop heat pipe for electric vehicle application. *Appl Therm Eng*. 2016;99:784–9. <https://doi.org/10.1016/j.applthermaleng.2016.01.123>.
 140. Putra N, Sandi AF, Ariantara B, Abdullah N, Indra Mahlia TM. Performance of beeswax phase change material (PCM) and heat pipe as passive battery cooling system for electric vehicles. *Case Stud Therm Eng*. 2020;21:100655. <https://doi.org/10.1016/j.csite.2020.100655>.
 141. Jiang ZY, Qu ZG. Lithium-ion battery thermal management using heat pipe and phase change material during discharge-charge cycle:

- a comprehensive numerical study. *Appl Energy*. 2019;242:378–92. <https://doi.org/10.1016/j.apenergy.2019.03.043>.
142. Zhang W, Qiu J, Yin X, Wang D. A novel heat pipe assisted separation type battery thermal management system based on phase change material. *Appl Therm Eng*. 2020;165:114571.
 143. Amin M, Ariantara B, Putra N, Sandi AF, Abdullah NA. Thermal management of electric vehicle batteries using heat pipe and phase change materials. *ES Web Conf*. 2018;67:1–5.
 144. Lei S, Shi Y, Chen G. A lithium-ion battery-thermal-management design based on phase-change-material thermal storage and spray cooling. *Appl Therm Eng*. 2020;168:114792.
 145. Huang Q, Li X, Zhang G, Zhang J, He F, Li Y. Experimental investigation of the thermal performance of heat pipe assisted phase change material for battery thermal management system. *Appl Therm Eng*. 2018;141:1092–100. <https://doi.org/10.1016/j.applthermaleng.2018.06.048>.
 146. Zhao J, Rao Z, Liu C, Li Y. Experimental investigation on thermal performance of phase change material coupled with closed-loop oscillating heat pipe (PCM/CLOHP) used in thermal management. *Appl Therm Eng*. 2016;93:90–100. <https://doi.org/10.1016/j.applthermaleng.2015.09.018>.
 147. Chi RG, Rhi SH. Oscillating heat pipe cooling system of electric vehicle's Li-ion batteries with direct contact bottom cooling mode. *Energies*. 2019;12:1–14. <https://doi.org/10.3390/en12091698>.
 148. Rao Z, Huo Y, Liu X. Experimental study of an OHP-cooled thermal management system for electric vehicle power battery. *Exp Therm Fluid Sci*. 2014;57:20–6. <https://doi.org/10.1016/j.expthermflusci.2014.03.017>.
 149. Wang Q, Rao Z, Huo Y, Wang S. Thermal performance of phase change material/oscillating heat pipe-based battery thermal management system. *Int J Therm Sci*. 2016;102:9–16. <https://doi.org/10.1016/j.ijthermalsci.2015.11.005>.
 150. Wei A, Qu J, Qiu H, Wang C, Cao G. Heat transfer characteristics of plug-in oscillating heat pipe with binary-fluid mixtures for electric vehicle battery thermal management. *Int J Heat Mass Transf*. 2019;135:746–60. <https://doi.org/10.1016/j.ijheatmasstransfer.2019.02.021>.
 151. Dan D, Yao C, Zhang Y, Zhang H, Zeng Z, Xu X. Dynamic thermal behavior of micro heat pipe array-air cooling battery thermal management system based on thermal network model. *Appl Therm Eng*. 2019;162:114183.
 152. Wan C. Thermal performance of heat pipe array in battery thermal management. *Teh Vjesn*. 2020;27:423–8.
 153. Wan C. Enhancement on the thermal behavior using heat pipe arrays in battery thermal management compared to cooper rods. *Therm Sci*. 2020;24:124–124. <https://doi.org/10.2298/tsci191210124w>.
 154. Liang J, Gan Y, Li Y, Tan M, Wang J. Thermal and electrochemical performance of a serially connected battery module using a heat pipe-based thermal management system under different coolant temperatures. *Energy*. 2019;189:116233.
 155. Gan Y, He L, Liang J, Tan M, Xiong T, Li Y. A numerical study on the performance of a thermal management system for a battery pack with cylindrical cells based on heat pipes. *Appl Therm Eng*. 2020;179:115740.
 156. Wang J, Gan Y, Liang J, Tan M, Li Y. Sensitivity analysis of factors influencing a heat pipe-based thermal management system for a battery module with cylindrical cells. *Appl Therm Eng*. 2019;151:475–85. <https://doi.org/10.1016/j.applthermaleng.2019.02.036>.
 157. Huang J, Shoai Naini S, Miller R, Rizzo D, Sebeck K, Shurin S, et al. Development of a heat pipe-based battery thermal management system for hybrid electric vehicles. *Proc Inst Mech Eng Part D J Automob Eng*. 2020;234:1532–43. <https://doi.org/10.1177/0954407019899588>.
 158. Li Y, Qi F, Guo H, Guo Z, Xu G, Liu J. Numerical investigation of thermal runaway propagation in a Li-ion battery module using the heat pipe cooling system. *Numer Heat Transf Part A Appl*. 2019;75:183–99. <https://doi.org/10.1080/10407782.2019.1580956>.
 159. Greco A, Cao D, Jiang X, Yang H. A theoretical and computational study of lithium-ion battery thermal management for electric vehicles using heat pipes. *J Power Sources*. 2014;257:344–55. <https://doi.org/10.1016/j.jpowsour.2014.02.004>.
 160. Murashko K, Pyrhönen J, Laurila L. Optimization of the passive thermal control system of a lithium-ion battery with heat pipes embedded in an aluminum plate. In 2013 15th European Conference on Power Electronics and Applications, 2013:1–10
 161. Yuan W, Yan Z, Tan Z, Chen W, Tang Y. Heat-pipe-based thermal management and temperature characteristics of Li-ion batteries. *Can J Chem Eng*. 2016;94:1901–8. <https://doi.org/10.1002/cjce.22566>.
 162. Zhou H, Zhou F, Xu L, Kong J. Thermal performance of cylindrical lithium-ion battery thermal management system based on air distribution pipe. *Int J Heat Mass Transf*. 2019;131:984–98.
 163. Sun X, Xu X, Tang W, Jin HDH. Research on multi-stage heating method of high-speed railway emergency traction battery system based on flat heat pipe. *Therm Sci* 2020:172.
 164. Zhang C, Xia Z, Wang B, Gao H, Chen S, Zong S, et al. A Li-ion battery thermal management system combining a heat pipe and thermoelectric cooler. *Energies*. 2020;13(4):841. <https://doi.org/10.3390/en13040841>.
 165. Shah K, McKee C, Chalise D, Jain A. Experimental and numerical investigation of core cooling of Li-ion cells using heat pipes. *Energy*. 2016;113:852–60. <https://doi.org/10.1016/j.energy.2016.07.076>.
 166. Behi H, Karimi D, Behi M, Ghanbarpour M, Jaguemont J, Sokkeh MA, et al. A new concept of thermal management system in Li-ion battery using air cooling and heat pipe for electric vehicles. *Appl Therm Eng*. 2020;174:115280.
 167. Wei T, Xiaoming X, Hua D, Yaohua G, Jicheng L, Hongchao W. Sensitivity analysis of the battery thermal management system with a reciprocating cooling strategy combined with a flat heat pipe. *ACS Omega*. 2020;5:8258–67. <https://doi.org/10.1021/acsomega.0c00552>.
 168. Xu X, Tang W, Fu J, Li R, Sun X. Plate flat heat pipe and liquid-cooled coupled multistage heat dissipation system of Li-ion battery. *Int J Energy Res*. 2019;43:1133–41. <https://doi.org/10.1002/er.4341>.
 169. Zhang Z, Wei K. Experimental and numerical study of a passive thermal management system using flat heat pipes for lithium-ion batteries. *Appl Therm Eng*. 2020;166:114660.
 170. Mousavi S, Zadehkabir A, Siavashi M, Yang X. An improved hybrid thermal management system for prismatic Li-ion batteries integrated with mini-channel and phase change materials. *Appl Energy*. 2023;334:120643.
 171. Zhang Z, Zhao R, Zhao S, Zou H, Liu Z, Luo X et al. Performance characteristics of a two-phase pump-assisted loop heat pipe with dual-evaporators in parallel. *Therm Sci Eng Prog* 2023:101657.
 172. Guo H, Ji X, Gan Y, Xu J. Experimental study on the heat transfer performance of loop heat pipe with different particle morphology and wettability of porous wick. *Int J Therm Sci*. 2023;186:108134.

Publisher's Note Springer Nature remains neutral with regard to jurisdictional claims in published maps and institutional affiliations.

Springer Nature or its licensor (e.g. a society or other partner) holds exclusive rights to this article under a publishing agreement with the author(s) or other rightsholder(s); author self-archiving of the accepted manuscript version of this article is solely governed by the terms of such publishing agreement and applicable law.